JGR Solid Earth

RESEARCH ARTICLE
10.1029/2018JB017120

Earthquake Declustering Using the Nearest-Neighbor Approach in Space-Time-Magnitude Domain

Ilya Zaliapin[1] and **Yehuda Ben-Zion**[2]

[1]Department of Mathematics and Statistics, University of Nevada, Reno, Reno, NV, USA, [2]Department of Earth Sciences, University of Southern California, Los Angeles, CA, USA

Key Points:
- A new declustering method is proposed based on nearest-neighbor analysis of earthquakes in time-space-magnitude domain
- Declustering the examined catalogs with magnitude range $\Delta m < 4$ leads to a stationary field with independent space-time components
- Declustering data with $\Delta m > 4$ reveal nonstationary patterns attributed to the original catalog rather than the method

Supporting Information:
- Supporting Information S1
- Data Set S1
- Data Set S2

Correspondence to:
I. Zaliapin,
zal@unr.edu

Citation:
Zaliapin, I., & Ben-Zion, Y. (2020). Earthquake declustering using the nearest-neighbor approach in space-time-magnitude domain. *Journal of Geophysical Research: Solid Earth*, *125*, e2018JB017120. https://doi.org/10.1029/2018JB017120

Received 1 DEC 2018
Accepted 17 JAN 2020
Accepted article online 22 JAN 2020

Abstract We introduce an algorithm for declustering earthquake catalogs based on the nearest-neighbor analysis of seismicity. The algorithm discriminates between background and clustered events by random thinning that removes events according to a space-varying threshold. The threshold is estimated using randomized-reshuffled catalogs that are stationary, have independent space and time components, and preserve the space distribution of the original catalog. Analysis of catalog produced by the Epidemic Type Aftershock Sequence model demonstrates that the algorithm correctly classifies over 80% of background and clustered events, correctly reconstructs the stationary and space-dependent background intensity, and shows high stability with respect to random realizations (over 75% of events have the same estimated type in over 90% of random realizations). The declustering algorithm is applied to the global Northern California Earthquake Data Center catalog with magnitudes $m \geq 4$ during 2000–2015; a Southern California catalog with $m \geq 2.5$, 3.5 during 1981–2017; an area around the 1992 Landers rupture zone with $m \geq 0.0$ during 1981–2015; and the Parkfield segment of San Andreas fault with $m \geq 1.0$ during 1984–2014. The null hypotheses of stationarity and space-time independence are not rejected by several tests applied to the estimated background events of the global and Southern California catalogs with magnitude ranges $\Delta m < 4$. However, both hypotheses are rejected for catalogs with larger range of magnitudes $\Delta m > 4$. The deviations from the nulls are mainly due to local temporal fluctuations of seismicity and activity switching among subregions; they can be traced back to the original catalogs and represent genuine features of background seismicity.

1. Introduction

Earthquakes are associated with various forms of clusters in space, time, and size that produce nonstationary complex event patterns (e.g., Ben-Zion, 2008, section 2, and references therein). Earthquake clustering is manifested most clearly by aftershock sequences consisting of numerous smaller events (aftershocks) following a larger earthquake (mainshock) in its space-time proximity (e.g., Kisslinger, 1996; Omori, 1894; Shcherbakov et al., 2005; Utsu & Ogata, 1995). Foreshocks are a related form of clustering involving pre-mainshock events associated with smaller number and smaller areas than those for aftershocks (e.g., Ellsworth, 2019; Jones, 1985; Mignan, 2014; Ogata et al., 1995; Seif et al., 2019). Foreshocks-mainshock-aftershock sequences are assumed to be related causally through triggering by dynamic, static, and longer-term postseismic stress-transfer mechanisms (e.g., Ben-Zion et al., 1993; Hill et al., 1993; King & Cocco, 2001). An example of a prominent aftershock sequence of the 1992 $m = 7.3$ Landers earthquake in Southern California is illustrated in Figure 1. Swarms are another general type of clustering involving a group of neighboring earthquakes with comparable size; they are assumed to be associated with triggering by aseismic deformation and/or migration of fluids (e.g., Hainzl, 2004; Hill, 1977; Lohman & McGuire, 2007; McGuire, 2019). Swarms occur generally in areas with elevated fluid-temperature conditions and low effective viscosity, whereas classical mainshock-aftershock sequences tend to occur in relatively cold high viscosity regions (Ben-Zion & Lyakhovsky, 2006; Zaliapin & Ben-Zion, 2016a). Oil and gas production, exploration of geothermal energy, and other anthropogenic activities can also lead to and modify observed forms of earthquake clustering (e.g., Ellsworth, 2013; Goebel & Brodsky, 2018; Martínez-Garzón et al., 2018; Schoenball et al., 2015).

In various problems, it is important to have declustered catalogs that do not include aftershocks, foreshocks, swarms, and other clear forms of clustered seismicity. Examples include efforts to clarify basic aspects of earthquake occurrence (e.g., Gardner & Knopoff, 1974); detection of tidal, seasonal, and climatic triggering of seismicity (e.g., Amos et al., 2014; Cochran et al., 2004; Gao et al., 2000; Hammond et al., 2019; Johnson

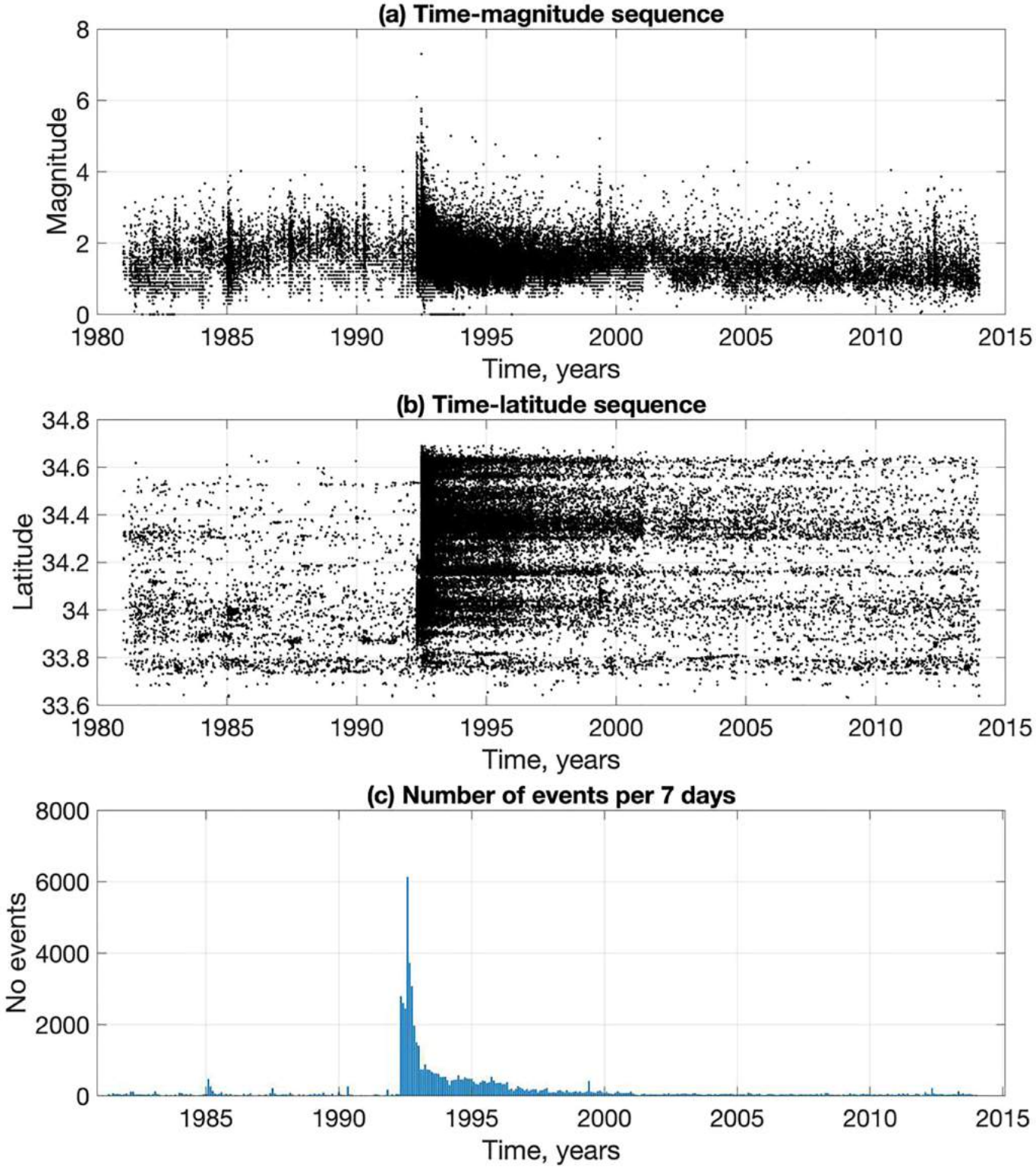

Figure 1. The aftershock sequence of Landers earthquake, 28 June 1992, $m = 7.3$. Catalog of Hauksson et al. (2012); 66,682 earthquakes with $m \geq 0.0$. (a) Time-magnitude sequence. (b) Time-latitude sequence. (c) Number of events in nonoverlapping time windows of 7 days. The aftershock sequence disturbs the entire seismic field for decades, affecting its intensity and space distribution.

et al., 2017, 2019); inversions of focal mechanisms for the background stress (e.g., Abolfathian et al., 2019; Martínez-Garzón et al., 2016); and seismic hazard estimates (e.g., Petersen et al., 2015, 2018). At present, there is no physical criterion that can separate independent (background) earthquakes from dependent (triggered) ones, and the desired form of a declustered catalog may depend on the application at hand. In some cases, like stress inversions of focal mechanisms, it is useful to retain the largest number of background events likely to be produced by the remote tectonic loading and remove triggered seismicity generated by stress transfers between events. In other cases, like evaluating long-range spatial seismic rates or earthquake-related rock damage, it may be useful to have a declustered version of the catalog with seismicity rate following closely that of a stationary Poisson process.

The early method of earthquake declustering by Gardner and Knopoff (1974) involves removing (i.e., classifying as clustered) all events that occur within a given space-time magnitude-dependent window around another earthquake. Several alternative window sizes were suggested in later studies (see van Stiphout et al., 2012, section 5.1, for a summary). This basic method inspired several generations of researchers aiming to discriminate between background and dependent earthquakes and quantify the degree of nonrandomness in the estimated background events. Notably, Gardner and Knopoff (1974) hypothesized that events in a properly declustered catalog follow a stationary Poisson process. Reasenberg (1985) proposed a more elaborate declustering algorithm based on connecting events in clusters according to adaptive space-time interaction zones and suggested that both the space and time marginal components of a proper background field are Poissonian. These two methods defined the paradigm of declustering (and related quality statistics) for decades and are still in common use (e.g., Petersen et al., 2018). Various later declustering methods have been developed using a range of assumptions and techniques. The algorithms of Davis and Frohlich (1991), Molchan and Dmitrieva (1992), Zhuang et al. (2002), Hainzl et al. (2006), Marsan and Lengline (2008), and Luen and Stark (2012) illustrate the diverse approaches to the declustering problem. We refer to Molchan and Dmitrieva (1992) and van Stiphout et al. (2012) for a historical and technical review of these and other declustering methods.

Luen and Stark (2012) revisited the problem of statistical analysis of declustered catalogs and suggested a statistical framework for testing the null hypothesis of a stationary Poisson process with independent space and time components. They observed that "*conclusions* [regarding Poisson behavior of a declustered catalog] *depend on the declustering method, the catalogue, the magnitude range, and the statistical test*." In particular, they showed (their Table 1) that declustered catalogs of Southern California with cutoff magnitudes m_c = 3.8, 4.0 by the methods of Gardner and Knopoff (1974) with several sets of parameters and Reasenberg (1985) produce inconclusive results according to more powerful statistical tests than those explored in the classical works. In other words, it is not clear if the obtained background seismicity follows a stationary Poisson field with independent space and time components even when using the same data, declustering techniques, and parameters, as in the works of Gardner and Knopoff (1974) and Reasenberg (1985). The declustering technique proposed in this work does not aim at producing a Poisson background (section 7); at the same time, it successfully reconstructs a stationary Poisson background in a model with known background properties (section 6).

The problem of detecting earthquake clusters (which is different from although closely related to declustering) was shown recently to be effectively addressed by a nearest-neighbor analysis in space-time-magnitude domain (Zaliapin et al., 2008; Zaliapin and Ben-Zion, 2013a, 2013b, 2015, 2016a, 2016b). This cluster identification methodology is effective in diverse settings, including tectonic seismicity (Gentili et al., 2017, 2019; Gu et al., 2013; Kossobokov & Nekrasova, 2017; Moradpour et al., 2014; Peresan & Gentili, 2018; Reverso et al., 2015; Ruhl et al., 2016; Trugman et al., 2017; Zaliapin et al., 2008; Zaliapin & Ben-Zion, 2013a, 2013b, 2016a), induced earthquakes (Goebel et al., 2019; Martínez-Garzón et al., 2018; Schoenball et al., 2015; Schoenball & Ellsworth, 2017; Teng & Baker, 2019; Vasylkivska & Huerta, 2017; Zaliapin & Ben-Zion, 2016b), synthetic seismicity in Epidemic Type Aftershock Sequence (ETAS) models (Gu et al., 2013; Zaliapin et al., 2008; Zaliapin & Ben-Zion, 2013a), and laboratory rock fracture experiments (Davidsen et al., 2017).

In this study we develop an earthquake declustering technique based on the nearest-neighbor earthquake approach. We adopt the testing methodology of Luen and Stark (2012) and consider additional time and space-time tests (section 5). When examining results based on our algorithm (section 6), the null hypothesis of a stationary background field with independent space and time components cannot be rejected for global seismicity with m_c = 5.0 and for Southern California seismicity with m_c = 3.5;

the range of examined magnitudes in these catalogs is roughly $\Delta m = 4$. In contrast, the same null hypothesis is strongly rejected when working with catalogs having lower cutoff magnitudes and hence wider range of event sizes $\Delta m > 4$. The observed deviations from stationarity and space-time independence are attributed to intrinsic nonhomogeneities of the seismicity flow and are unlikely to be pure artifacts of the declustering method.

The developed declustering approach features (i) simple parameterization—it has only three easily estimated parameters, (ii) weak sensitivity to parameter values and catalog uncertainties, and (iii) absence of ad hoc assumptions about cluster model and properties of the declustered field. The same main features have facilitated the nearest-neighbor approach for identification and analysis of earthquake clusters. The problem of declustering addressed in this work is different from that of cluster identification, despite a clear relation between the two. The principal difference is due to a substantial overlap between the spatiotemporal domains of aftershock sequences and background events. Specifically, multiple background events are likely to occur within the space-time domains occupied by aftershock sequences and can be misclassified as clustered. When the analysis focuses on properties of large clusters, this overlap has less impact because the number of correctly identified clustered events within a large cluster is much larger than the number of misclassified background events. In the declustering problem, however, missing even a small number of true background events can visibly distort the result. We further discuss this issue in section 3. This problem is well known and necessitates stochastic methods of declustering. For instance, Zhuang et al. (2002) estimated the probability for each earthquake in an examined catalog to belong to the background, assuming that earthquake clusters follow the ETAS model (Ogata, 1988, 1999, 2011). These background probabilities were then used to generate independent random partitions of events into background and triggered populations. This approach is based on a rigid assumption (ETAS model) regarding how earthquakes cluster; the success of the declustering is determined by the ability of the model to fit observations and ability of a user to correctly estimate multiple model parameters. Marsan and Lengline (2008) expanded this stochastic declustering idea to an arbitrary conditional intensity (i.e., arbitrary cluster model) that is parametrized by a piecewise constant function in space-time-magnitude domain and can be estimated using the expectation-minimization procedure.

The declustering algorithm proposed in the present study is also stochastic and uses random reshuffling and thinning of the examined catalog. The main difference with respect to Zhuang et al. (2002) and Marsan and Lengline (2008) is that these methods use an assumed cluster model (whose parameterization might be known as in the ETAS approach or unknown a priori as in the latter study) and then remove estimated clustered events. In contrast, our algorithm searches for deviations of the analyzed seismicity from a stationary field having independent space and time marginal components, with the space marginal taken from the observations. This eliminates the time-consuming and potentially biasing cluster model estimation step and naturally adapts to the observed fault network geometry and variability of local earthquake rates. The algorithm uses the nearest-neighbor proximities, taking advantage of their bimodal distribution (short for clustered events and long for background) that has been documented in previous studies (see section 3 and supporting information Figure S8). An abnormally short proximity increases the probability for event to belong to the cluster population. This approach expands possible forms of clustering aimed for detection and removal. Also, it generically allows for different types of clusters (i.e., different forms of conditional intensity) to exist at different times and space locations.

The reminder of the paper is organized as follows. Section 2 describes the earthquake catalogs used in the study. The nearest-neighbor earthquake proximity is reviewed in section 3. The proposed declustering algorithm is introduced in section 4. Section 5 describes the statistical testing framework for quantifying deviations of an estimated background field from stationarity and space-time independence. Section 6 applies the developed algorithm to synthetic seismicity of the ETAS model. This experiment allows us to compare the true and estimated classification of events into background and clustered populations and illustrates the efficiency of the proposed technique. The declustering algorithm is then applied to five observed catalogs in section 7. The results are discussed the section 8.

2. Data

We analyze global seismicity, earthquakes in California, and a synthetic catalog produced by the ETAS model. Table 1 summarizes information about the examined data.

Table 1
Earthquake Catalogs Examined in the Study

Catalog	Time period (duration, years)	Magnitude range (m_{max}–m_{min})	No. events	Intensity (events per day[a])	Reference	Section	Figures
ETAS	1–21.9 (20.9)	2.50–7. 33 (4.83)	26,986	3.54	Gu et al. (2013)	6	3–7
World	2000–2015 (15)	5.0–9.1 (4.1)	22,694	4.14	NCEDC (2016)	7.1	8 and 9
Southern California	1981–2017 (37)	2.5–7.3 (4.8)	43,633	3.23	Hauksson et al. (2012)	7.2	10 and 11
Southern California	1981–2017 (37)	3.5–7.3 (3.8)	4,125	0.31	Hauksson et al. (2012)	7.2	12 and 13
Landers	1981–2013 (33)	0.0–7.3 (7.3)	66,682	5.53	Hauksson et al. (2012)	7.3	14 and 15
Parkfield	1984–2010 (26)	1.0–6.0 (5.0)	8,648	0.91	Waldhauser and Schaff (2008)	7.4	16 and 17

[a]This intensity estimation is obtained by dividing the total number of reported events by the time duration.

2.1. Global Seismicity

The global analysis is based on the catalog produced by the Northern California Earthquake Data Center (NCEDC, 2016). We examine 22,694 events with magnitude $m \geq 5$ for the period 2000–2015. We only consider events with hypocentral depth less than 70 km. The depth reporting in NCEDC catalog is not accurate, and about 60% of the events are assigned discrete depth values of 35, 33, 30, 10, or 5 km. Our analysis is based on earthquake epicenters and is not affected by the depth uncertainties. The examined catalog contains two events with $m \geq 9$: Sumatra-Andaman earthquake of 26 December 2004, $m = 9.0$ (Lay et al., 2005), and Tohoku earthquake of 11 March 2011, $m = 9.1$ (Fujii et al., 2011). It also contains 17 earthquakes with $m \geq 8.0$. Each of these large earthquakes has a significant aftershock sequence. Analysis of cluster properties of $m \geq 4$ event in the NCEDC global catalog has been done by Zaliapin and Ben-Zion (2016a).

2.2. Seismicity of Southern California

In Southern California, we use the waveform-relocated catalog of Hauksson et al. (2012); an extension of this catalog to the interval 1981–2017 is available via the SCEC data center. The overall catalog completeness magnitude is between 2 and 3 (Zaliapin & Ben-Zion, 2013a) and may differ in space and time depending on the quality of seismic network. We consider events of all depths but only work with epicenters since the depths of earthquakes is generally less constrained than the horizontal locations. The examined catalog includes three earthquakes with $m \geq 7$: Landers earthquake of 28 June 1992, $m = 7.3$ (Hill et al., 1993); Hector Mine earthquake of 16 October 1999, $m = 7.1$ (Fialko et al., 2001); and El Mayor-Cucapah earthquake of 4 April 2010, $m = 7.2$ (Hauksson et al., 2011). We consider 43,633 events with $m \geq 2.5$ and 4,125 events with $m \geq 3.5$. Nearest-neighbor analyses of cluster properties of Southern California events in the Hauksson et al. (2012) and two alternative catalogs were done by Zaliapin and Ben-Zion (2013a, 2013b, 2015) and Gu et al. (2013).

2.3. Seismicity of Northern California

We analyze data in the Northern California relocated catalog of Waldhauser and Schaff (2008) and Schaff and Waldhauser (2005) that covers the Parkfield segment of the San Andreas fault. We use an updated version of the catalog for the period 1984–2010. The completeness magnitude in the examined region is about $m_c = 2.5$. The examined catalog includes one moderate event: the Parkfield earthquake of 28 September 2004, $m = 6.0$ (Langbein et al., 2005). We consider 8,648 events with $m \geq 1.0$ and only use epicentral locations of the earthquakes.

2.4. Synthetic Seismicity

We work with an ETAS catalog from Gu et al. (2013). This catalog has been generated using spatially variable background intensity and other parameters that closely fit those estimated for Southern California. The model uses a triggering kernel that is a product of its marginal time and space components. The time component decays in time according to the Omori-Utsu power law (Utsu & Ogata, 1995). The space component is isotropic and depends only on the distance r from the triggering event; for small r, it increases linearly with r, while for large r, it decreases as $r^{-1.6}$. A complete description of the model and the values of its parameters can be found in Gu et al. (2013, section 3); the catalog is available in the auxiliary materials of that paper. The smallest and largest magnitudes of the examined catalog are $m = 2.5$ and $m = 7.33$, respectively. The catalog

has 26,986 events, including five events with $m > 6$. A nearest-neighbor analysis of cluster properties of this catalog was done by Gu et al. (2013).

3. Nearest-Neighbor Proximity for Earthquakes

The key element of the proposed declustering algorithm (described in section 4) is the nearest-neighbor proximity between earthquakes in space-time-magnitude domain, which we review in this section. We refer to Zaliapin and Ben-Zion (2013a, 2015, 2016a) for comprehensive discussions of the proximity and respective nearest-neighbor cluster analyses of earthquakes.

Consider a catalog of earthquakes where each event i is characterized by its occurrence time t_i, hypocenter $\mathbf{x}_i = (\phi_i, \lambda_i, z_i)$, and magnitude m_i. The proximity of earthquake j to previous earthquake i is asymmetric in time and is defined as (Baiesi & Paczuski, 2004; Zaliapin et al., 2008)

$$\eta_{ij} = \begin{cases} t_{ij}\left(r_{ij}\right)^d 10^{-wm_i}, & t_{ij}>0; \\ \infty, & t_{ij}\leq 0. \end{cases} \tag{1}$$

Here, $t_{ij} = t_j - t_i$ is the event intercurrence time, which is positive if event j occurred after event i; $r_{ij} \geq 0$ is the spatial distance between the earthquake hypocenters (or epicenters); d is the fractal dimension of the hypocenters (or epicenters); and w is the parameter that introduces exponential weight of the earlier event i by its magnitude. In cluster analyses, this parameter usually equals the b value of the Gutenberg-Richter law that approximates the observed number $N(m)$ of events with magnitude above m:

$$\log_{10} N(m) = a - bm, \qquad b \approx 1, \qquad m \geq m_c. \tag{2}$$

In this study we work with epicenters of events. Intuitively, the earthquake proximity (1) is the expected number of events "between" the examined pair of earthquakes in a stationary process with independent space and time components (see Zaliapin & Ben-Zion, 2016b, Equation (4), for technical details).

For each event j, we identify its unique nearest neighbor (parent) i based on the proximity of equation (1) and denote the respective nearest-neighbor proximity by η_j:

$$\eta_j = \min\left(\eta_{ij}, i<j\right). \tag{3}$$

The event j is then called an offspring of i. According to this definition, each event (except the first in the catalog) has a unique parent and may have multiple offspring. The space and time distances between event j and its parent i normalized by the magnitude m_i of the parent event are (Zaliapin et al., 2008)

$$T_{ij} = t_{ij} 10^{-qwm_i}; \quad R_{ij} = \left(r_{ij}\right)^d 10^{-pwm_i}; \quad q + p = 1, \tag{4}$$

so $\log\eta_{ij} = \log T_{ij} + \log R_{ij}$. Zaliapin et al. (2008) and Zaliapin and Ben-Zion (2013a) demonstrated that a Poisson marked field with stationary time component, uniform or inhomogeneous random space component, and Gutenberg-Richter magnitude distribution corresponds to a unimodal distribution of ($\log_{10} T$, $\log_{10} R$) that is concentrated along a line $\log_{10} T + \log_{10} R = \text{const}$. On the other hand, observed seismicity follows a bimodal distribution of ($\log_{10} T$, $\log_{10} R$). One of the observed modes is similar to that in a Poisson field; it corresponds to *background* events. The other mode is located considerably closer in time and space to the origin; it corresponds to *clustered* events. This bimodality has been documented in multiple regions and on multiple scales (Gentili et al., 2017, 2019; Gu et al., 2013; Kossobokov & Nekrasova, 2017; Moradpour et al., 2014; Peresan & Gentili, 2018; Ruhl et al., 2016; Schoenball et al., 2015; Trugman et al., 2017; Vasylkivska & Huerta, 2017; Zaliapin & Ben-Zion, 2013a, 2013b, 2016a, 2016b). The bimodality of observed seismicity facilitates cluster detection and declustering.

Earthquake cluster analyses have been usually done with parameter w equal to the b value of the Gutenberg-Richter law, as defined by equation (2). With this choice, the multiplicative factor 10^{-wm} in the proximity of equation (1) increases the space-time domain of potential offspring of large-magnitude events, which is necessary for correct identification of their aftershock sequences. To illustrate this, we define the

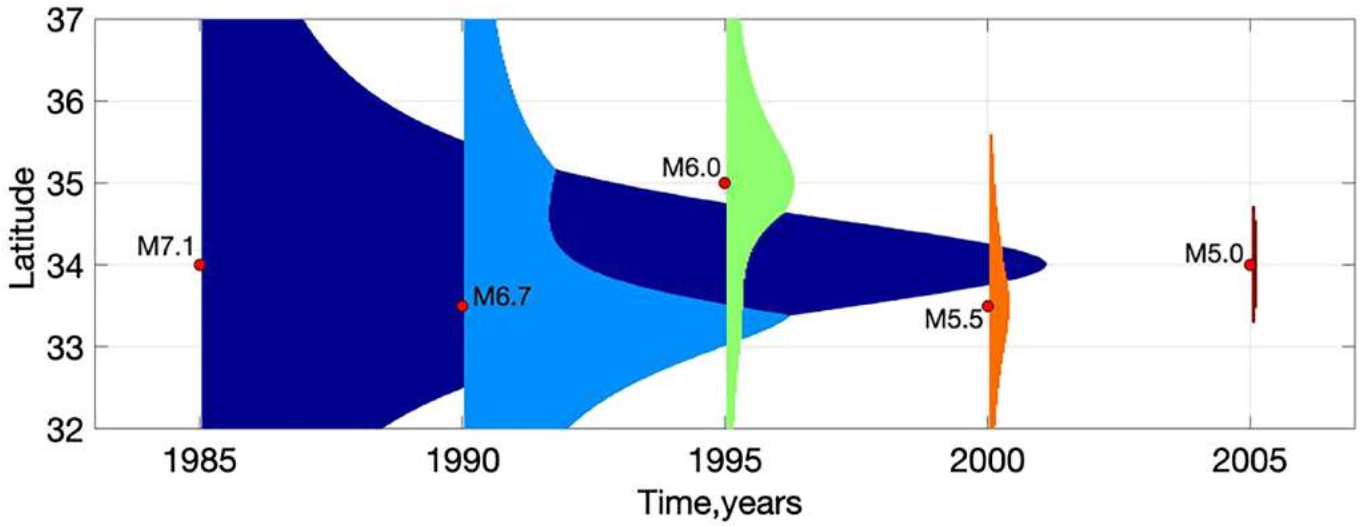

Figure 2. Attraction domains in a synthetic catalog of Table 2. The figure shows (by different colors) the time-latitude projections of attraction domains of earthquakes from the synthetic catalog. The attraction domains are defined by the condition $\eta_i < 10^{-2.75}$; the analysis parameters are $d = 1.6$ and $w = 1$. Notice exponential dependence of the domain size on event magnitude, which would make the domains of events with magnitude below M5 unnoticeable on this scale. The complex shape of the domain of M6.7, $t = 1990$ event is caused by the nearest-neighbor proximity competition with the domain of an earlier M7.1 event.

attraction domain of a given earthquake i as the set of the space-time locations $(\mathbf{x},t)$ whose nearest-neighbor proximity of equation (1) to event i is less than that to all other events in the catalog. Figure 2 illustrates the attraction domains of earthquakes in a synthetic catalog listed in Table 2. For visual convenience, the figure only shows the parts of the attraction domains that satisfy the condition $\eta_j < 10^{-2.75}$. The exponential dependence of the attraction domain on the event magnitude (i.e., the 10^{-wm} term) results in extremely heterogeneous distribution of domain sizes. For example, the attraction domain of an earthquake with $m = 7.1$, $t = 1985$ in Figure 2 occupies about a third of the examined space-time area, while the attraction domain of event $m = 5.0$, $t = 2005$ is so small that it is barely distinguishable in Figure 2.

The typical ratio of aftershock-to-background intensities is high within aftershock sequences. Hence, the number of background events that occur within the attraction domain of a large event and are incorrectly classified as aftershocks is small compared to the number of true aftershocks in this domain. Therefore, this misclassification does not contaminate cluster detection and analyses. A detailed qualitative assessment of this artifact was done in Zaliapin and Ben-Zion (2013a) using synthetic and real catalogs. For the declustering problem, however, mistakenly removing even a relatively small number of background events can have an adverse effect on the overall result. As an example, the proportion of background events with magnitude $m \geq 0.0$ in the area around the Landers aftershock series (section 7.3 and Figures 1 and 14) during the entire period (>30 years) covered by the catalog is only about 2% of the total reported number (over 60 K) of events. Clearly, including these background events in the aftershock sequence will not bias the aftershock cluster statistics. However, excluding these events from the background field can cause a notable deficiency in the declustered catalog. Specifically, this produces holes (space-time domains with no earthquakes), similar to those commonly produced by window declustering techniques. The illustration of attraction domains in Figure 2 suggests that this effect is particularly strong after large earthquakes (as is the case for the Landers aftershock sequence). This motivates us to use $w = 0$ in the declustering analysis introduced in the next section. The proximity (1) calculated with $w = 0$ preserves the bimodality observed for $w = 1$ while deflating the attraction domains of large earthquakes. The combination of these properties is very useful for declustering.

Table 2
Synthetic Catalog Used to Illustrate Domain of Attraction in Figure 2

Time	Latitude	Longitude	Magnitude
1985	34.0	−121.0	7.1
1990	33.5	−121.0	6.7
1995	35.0	−121.0	6.0
2000	33.5	−121.0	5.5
2005	34.0	−121.0	5.0

4. Declustering Algorithm

The proposed declustering algorithm uses the earthquake nearest-neighbor proximity η_j of equations (1) and (3) to separate clustered and

background events. Roughly speaking, we think of events with small η_j (close to the parent) as clustered and events with large η_j (far from the parent) as background. This coarse classification, which is used in the cluster analysis (see references in section 1), is refined here to preserve spatially varying background levels and reconstruct background events within the attraction domains of large earthquakes. The first goal is achieved by randomized-reshuffled catalog analysis and the second by random thinning.

4.1. Description of Declustering Algorithm

Consider a catalog of events

$$C_0 = \{t_i, \mathbf{x}_i, m_i\}, i = 1, ..., N,$$

where each event is specified by its occurrence time t_i, spatial coordinate $\mathbf{x}_i$ (which can be either two- or three-dimensional), and magnitude m_i. For each event i in the catalog, we define its nearest-neighbor proximity η_i according to equations (1) and (3). We use $w = 0$ to reduce artifacts related to the overlap of the earthquakes' domain of attraction with background seismicity (see section 3 and Figure 2). The magnitude is retained in the description of the algorithm, so it can be used with an arbitrary w if needed.

The proposed declustering is done in the following four steps:

Step 1. Identify the most clustered events. This step coincides with identification of clustered events used in the nearest-neighbor cluster analysis of seismicity (see Zaliapin & Ben-Zion, 2013a, and other references in section 3); it involves a single parameter η_0. The proposed declustering methodology goes beyond this crude assessment (see Steps 2–4), and hence, the final background intensity, estimated in Step 4, may not coincide with the estimation of Step 1.

Step 2. Coarsely estimate the relative location-specific background intensity at the location of each event i. This step uses randomized-reshuffled catalogs that exclude the most clustered events found in Step 1.

Step 3. Calculate the *normalized* nearest-neighbor proximity α_i for each event, by scaling the original nearest-neighbor proximity η_i according to the estimated background intensities of Step 2. Ideally, the normalized proximity has the same distribution at all locations.

Step 4. Apply thinning (random removal) to the events of the original catalog with a thinning probability that depends on the normalized proximity α_i. The remaining events comprise the declustered catalog. This step involves a single threshold parameter α_0.

Next, we describe the details of each step.

Step 1. We observe that the spatial pattern of aftershocks follows closely the fault geometry of the largest mainshocks. Therefore, it may not coincide with the spatial pattern of the background seismicity, which is more distributed and mainly comprised of small-to-intermediate events. Accordingly, we exclude the most clustered events (which are very likely aftershocks) from estimation of the location-specific background intensity levels. For that, we fix a cutoff proximity η_0 and only consider events with the nearest-neighbor proximity $\eta_i > \eta_0$. We denote by N_0 the number of events in the original catalog that satisfy this condition. Formally, we identify the sequence of $N_0 \le N$ indices $i(1)$, ... , $i(N_0)$ such that

$$\left\{ i(j) : \eta_{i(j)} > \eta_0 \right\}, j = 1, ..., N_0. \tag{5}$$

Step 2. The estimation of the relative location-specific background intensity is done using randomized-reshuffled catalog analysis. We use the events with indices $i(1)$, ... , $i(N_0)$ identified in Step 1 to generate M randomized-reshuffled catalogs

$$C_k = \left\{ u_j, \mathbf{x}_{i(j)}, m_{i(\pi(j))} \right\}, j = 1, ..., N_0, k = 1, ..., M \tag{6}$$

for a significantly large number M of uniform random permutations π on $\{1, ... , N_0\}$. The spatial locations $\mathbf{x}_{i(j)}$ of events in these catalogs are taken from the original catalog C_0. The random times u_j are drawn from the uniform distribution on the time domain $[\min(t_i), \max(t_i)]$ of the original catalog C_0. Each randomized-

reshuffled catalog is composed of N_0 events with a stationary Poisson time component and independent space and time marginal distributions; each catalog preserves the spatial distribution of the events from the original catalog that satisfy the condition $\eta_i > \eta_0$.

Next, for every event i in the original catalog C_0, we find its nearest-neighbor proximity $\kappa_{k,i}$ with respect to the events from the kth randomized catalog C_k. These proximities comprise vector

$$\boldsymbol{k}_i = \left(\kappa_{1,i}, ..., \kappa_{M,i}\right), i = 1, ..., N.$$

The empirical distribution of components in the vector $\boldsymbol{k}_i$ approximates the nearest-neighbor proximity that would be observed for event i in a catalog with no clustering. This distribution shifts to the right (higher values) in regions with low background intensity and to the left (lower values) in regions with high background intensity.

Step 3. Next, we normalize the proximities η_i (calculated using the original catalog) according to the location-specific intensity levels given by vectors $\boldsymbol{k}_i$. This allows us in Step 4 to apply a common thinning procedure to regions with different background rates. To be less affected by data outliers, we consider the logarithmic proximity $\log_{10}[\eta_i]$ and correct it according to the estimated location-specific background intensity $mean[\log_{10}(\boldsymbol{k}_i)]$. Here the operator $mean[\boldsymbol{z}]$ denotes taking the sample average of the elements of vector $\boldsymbol{z}$. This defines the normalized proximity α_i such that

$$\log_{10}[\alpha_i] = \log_{10}[\eta_i] - mean[\log_{10}(\boldsymbol{k}_i)], i = 1, ..., N. \quad (7)$$

The normalization (7) accounts for possible inhomogeneities of the spatial intensity of background events that is quantified here by a space-dependent distribution of $\boldsymbol{k}_i$.

Step 4. The normalized proximities α_i are used to classify the events in the catalog C_0 into background and clustered. Intuitively, a background event can be defined as event with normalized proximity α_i above a threshold. This thresholding respects space-varying background levels according to the normalization (7). An explicit threshold procedure, however, may leave holes in the declustered catalog in the vicinity of the largest events (the size of the holes increases with w, as discussed in section 3). To eliminate such holes, we add random thinning—another stochastic component of the algorithm. The goal of the thinning is to retain some of the events with short normalized proximities. This simulates the occurrence of background events that would have occurred within the space-time domains currently occupied by aftershock sequences and hence fills the holes associated with the overlap of the attraction domains and the background field.

Formally, we define the probability $P_{\text{back},i}$ for event i to be identified as a background event:

$$P_{\text{back},i} = \min\{\alpha_i A_0, 1\}, \quad (8)$$

where the constant A_0 serves as a cluster threshold (or, formally speaking, inverse threshold). The number of events recognized as background increases with A_0. In the procedure defined by (8), events with large normalized proximities, $\alpha_i > 1/A_0$, are always recognized as background. The events with low normalized proximities $\alpha_i < 1/A_0$ are randomly thinned; the probability to be identified as a background event (and hence to be retained in a declustered catalog) equals $\alpha_i A_0$. Below we work with logarithmic form of proximities, $\log_{10}[\alpha_i]$, and, accordingly, use the logarithmic threshold $\alpha_0 = \log_{10}[A_0]$.

In a numerical implementation, event i is identified as a background event if the following condition is satisfied:

$$\alpha_i A_0 > U_i, \quad (9)$$

where U_i is a set of independent identically distributed (i.i.d.) uniform random variables on the interval [0, 1].

A theoretical motivation for the proposed algorithm, using distribution results for the nearest-neighbor proximity in a Poisson point field and general theory of thinning for point processes (Clements et al., 2012; Daley & Vere-Jones, 2003, 2008; Møller & Schoenberg, 2010; Schoenberg, 2003), is provided in the section S1. In particular, we notice that the nearest-neighbor proximities η_i in a Poisson process with no clustering are well approximated by Weibull distribution with location-specific mean. This corresponds to Gumbel distribution of $\log_{10}\eta_i$. The properties of Gumbel distribution justify the normalization (7) that removes the dependence on spatial location, making the distribution of α_i to be the same at all locations (given that the initial catalog has no clusters). The existence of clusters inflates the left tail of the distribution of α_i—this heavy tail is removed by random thinning of Step 4. Section S1 also shows that the proposed thinning is a natural extension of process-depending thinning in one dimension (Daley & Vere-Jones, 2008) to a multidimensional setting. Section S2 outlines the main steps in a numerical implementation of the algorithm.

The above declustering procedure can be slightly modified, to reflect the foreshock-mainshock-aftershock representation of seismic sequences. Observe that the parent links (section 3) connect all events in the examined catalog into a spanning time-oriented tree. By removing the parent links of the background events, we partition the catalog into a set of clusters, each of which is represented by a time-oriented tree that starts at a background event (root). The declustered catalog discussed above retains the first event from every cluster. This choice is natural when magnitude or time of events in a declustered catalog is ignored. This happens, for example, in assessing homogeneity of the space-time distribution of epicenters (magnitude is ignored) or in estimating long-term spatial intensity of background events (time and magnitude are ignored). Alternatively, one can decide to keep the largest earthquake from every cluster. This approach ensures, for instance, that the largest catalog events are treated as background. The differences between the space-time distributions of declustered events in these two approaches are minimal, since the space-time separation between the first and the largest event in a cluster is typically small compared to separation between clusters. The selection of a single event from each cluster (to be classified as background) depends on the problem at hand. The illustrations in this work show the first event in a cluster.

4.2. Parameters of Declustering Algorithm

The proposed algorithm has three numerical parameters: the fractal dimension of epicenters/hypocenters d used in the proximity equation (1); the initial cutoff proximity η_0 of Step 1, equation (5); and the cluster threshold α_0 of Step 4, equation (8). In general, it is possible to apply the algorithm with a nonzero value of w (an exponential weight applied to parent magnitudes) in which case the number of parameters increases to four.

4.2.1. Parameters d and w of the Proximity

It has been shown in Zaliapin and Ben-Zion (2013a) that the nearest-neighbor analysis is very stable with respect to d and w. This stability is inherited by the declustering algorithm. The fractal dimension of earthquake epicenters (hypocenters) is normally a fractional number within the interval [1, 2] ([2, 3]). We recommend using a fractal dimension d estimated for the actual set of earthquakes being examined. In the absence of such an estimation, we recommend using the midrange value $d = 1.5$ for epicenters and $d = 2.5$ for hypocenters. The declustered catalogs with similar alternative values of d do not differ much. We suggest using $w = 0$ for declustering for the reasons discussed in section 3. All results presented in this paper are based on $w = 0$.

4.2.2. Initial Cutoff Threshold η_0

The initial cutoff proximity threshold η_0 is used in Step 1 to select events for a rough evaluation of the relative space-dependent intensity of the background events (see equation (5)). Importantly, the only goal of Steps 1 and 2 is to estimate the relative local intensity (i.e., the value of intensity up to a multiplicative constant), not the absolute one, which is controlled by the cluster threshold α_0 of Step 4. Ideally, the threshold η_0 should separate the intensity (in year^{-1} km^{-2}) of background and clustered events. Accordingly, the choice of η_0 does not significantly affect the declustered catalog if this threshold is (i) large enough to eliminate prominent clusters that contain a large number of events and (ii) small enough to retain a sufficient number of events in the low-intensity regions. Given the focus on the relative background intensity, cutting out a part of the background (when η_0 is large) is less problematic that keeping large clusters (when η_0 is small). This implies that the value of η_0 is mostly affected by the upper boundary of the intensity of clustered events. At the same time, the threshold is not affected, in general, by the time duration or spatial extent of the examined catalog.

The declustering results become sensitive to the value of η_0 if the catalog is dominated by aftershocks of a very small number of mainshocks. An example is given in section 7.3 that examines the aftershock sequence of the $m = 7.3$ Landers earthquake. Over 97% of the events in the examined catalog are aftershocks of the Landers earthquake (according to any reasonable analysis), and using them to evaluate relative background intensity may substantially affect the result. In this situation, the declustered catalog is more sensitive to the initial threshold η_0.

The analyses of sections 6 and 7 show that the value $\eta_0 = 10^{-1}$ works efficiently in the global catalog with $m_c = 5.0$; in Southern California with $m_c = 2.5$ and 3.5, which corresponds to a tenfold difference in the number of examined events; for the Landers aftershock sequence with $m_c = 0$; and for the ETAS model with parameters fitted for Southern California. In some cases, however, an alternative threshold is needed; we illustrate this in the Parkfield segment of San Andreas fault where $\eta_0 = 10^{-2.5}$ works well (section 7.4).

A data-specific η_0 threshold can be selected using the bimodality of the distribution of earthquake nearest-neighbor proximities η_i. An automated threshold selection can be performed using a Gaussian mixture model (e.g., Zaliapin & Ben-Zion, 2016a, Section 3.4).

4.2.3. Cluster Threshold α_0

The declustering is most sensitive to the cluster threshold α_0—this parameter directly controls the number of background events in a declustered catalog. Importantly, the cluster threshold does not substantially affect the relative spatial intensity of background events, which is primarily controlled by the threshold η_0 of Step 1; it only affects the overall background intensity.

To suggest a reasonable range of values for α_0, we notice that in a case of a Poisson time-stationary and space-inhomogeneous catalog, the normalized logarithmic proximities $\log_{10}[\alpha_i]$ are concentrated around zero. Indeed, if one uses all events for reshuffling (i.e., $\eta_0 = 0$), then the Poisson model is statistically equivalent to its randomized-reshuffled version. This implies, in particular, that $E[\log_{10}(\kappa_{k,i})] = E[\log_{10}(\eta_i)]$ for an arbitrary realization k of reshuffling and any event index i. Here $E[]$ denotes the expected value with respect to the Poisson process. Applying now the expectation operator to equation (7), we find

$$E[\log_{10}(\alpha_i)] = E[\log_{10}(\eta_i)] - E\left[\log_{10}\left(\kappa_{k,i}\right)\right] = 0. \tag{10}$$

Here we used the linearity of operators $E[]$ and $mean[]$:

$$E[mean[\log_{10}(\boldsymbol{k}_i)]] = mean[E[\log_{10}(\boldsymbol{k}_i)]] = E\left[\log_{10}\left(\kappa_{k,i}\right)\right] \text{ for arbitrary } k.$$

In agreement with this argument, all modeled and real catalogs examined in this work have the normalized logarithmic proximities $\log_{10}[\alpha_i]$ concentrated around zero. We therefore recommend, in a search for an optimal declustered catalog, to explore α_0 around zero. For example, one can start with $-1 \le \alpha_0 \le 1$ and expand it if needed.

4.3. Possibility of a Nonstationary Declustered Field

The randomized-reshuffled catalogs of Step 2, equation (6) in section 4.1, that are used to estimate local background intensity are necessarily stationary in time. This, however, does not imply stationarity of the declustered catalog. This is because application of an upper intensity threshold to seismicity at a given location (Step 4 in section 4.1) does not imply a constant resulting intensity. To illustrate this, consider the following simple example. A cluster point process (no space and magnitude components) is composed of background with intensity 1 event per day during the interval 0–10 years and intensity 2 events per day during 10–20 years. In addition, a cluster follows each background event for 6 hr (1/4 of a day) with intensity 100 events per day; hence, each cluster consists of about 26 events (one mainshock and an average of 100/4 = 25 aftershocks). This process has a clear separation between the background and cluster intensities. Applying an upper intensity threshold of, for example, 10 events per day removes (most of) the clustered events. However, this threshold preserves the time-varying background intensity. The same principle works in the proposed algorithm—we remove clustered events while preserving the intensity of nonclustered ones, which might be nonstationary. We demonstrate this effect with real data in section 7.

5. Quantifying Spatiotemporal Fluctuations of a Declustered Catalog

The proposed algorithm of section 4 aims at eliminating events that occur abnormally close to their nearest neighbors, hence suggesting causal dependence. The algorithm, however, does not have a goal of producing a Poissonian declustered catalog (see section 4.3). Accordingly, the estimated background field may or may not be stationary in time and may or may not have spatiotemporal-dependent patterns. Any remaining deviations from time-stationary- and space-time-independent Poisson point field may provide information about regional loading processes and are worth of further analysis. We use here two types of statistics (and related tests) to quantify space-time fluctuations in the declustered earthquake field. The first type is aimed at testing the null hypothesis of a time-stationary Poisson process; it only uses times of events and ignores their spatial locations. The second type tests a more complex null hypothesis of independence between space and time coordinates of events; it uses both times and locations of earthquakes. Using a collection of complementary tests is important for objective assessment of declustering quality, especially in a situation when we do not assume a particular model of background flow (see also Luen & Stark, 2012). In this work we use five tests, three temporal tests, and two space-time tests, which are described in the next section.

5.1. Tests of Stationarity in Time

The tests and statistics considered in this section quantify deviations from a time-stationary Poisson process. Formally, we test the null hypothesis H_0: *The time sequence of events comes from a stationary Poisson process.*

5.1.1. The Bridge Test

This test examines the deviation in the cumulative number of events from that expected in a stationary Poisson process with the same total number of events. We start with a general setup. Consider a point process P that describes the temporal history of seismicity in a given region. Let $P(I)$ denote the number of events that occurred within the time interval I. We focus on deviations of $P(I)$ from its expected value $E[P(I)]$. For a stationary Poisson process with intensity μ (events $\times$ year^{-1}), the random variable $P([0,t])$ has the Poisson distribution with parameter μt (events). Specifically, for any integer $k \geq 0$, we have

$$\text{Prob}[P([0,t]) = k] = \exp(-\mu t)(\mu t)^k/k! \tag{11}$$

Accordingly, the expected number of events within the interval $[0, t]$ is given by a linear function with slope μ:

$$E[P([0,t])] = \mu t. \tag{12}$$

The intensity μ is generally unknown. The Maximum Likelihood Estimation (MLE) for μ is given by the observed rate of events in the interval $[0, T]$:

$$\mu_{MLE} = P([0,T])/T = N/T, \tag{13}$$

where $N = P([0,T])$ is the total observed number of events. The bridge $B(t)$ is defined as the deviations of the process P from its estimated mean, conditioned on the total number N of events. Replacing μ in equation (12) with μ_{MLE} of equation (13), we obtain

$$B(t) = P([0,t]) - E[P([0,t])] = P([0,t]) - Nt/T. \tag{14}$$

By definition, $B(0) = B(T) = 0$ and $E[B(t)] = 0$ for any instant t in $[0, T]$. The variance of the bridge for a stationary Poisson process with N events within $[0, T]$ is given by

$$Var[B(t)] = Nt(T-t)/T^2. \tag{15}$$

To remove the explicit dependence of the variance on the total number of events N and interval duration T, we consider the normalized deviation of the process from its mean value:

$$\Delta(t) = \frac{B(t)}{\sqrt{Var[B(t)]}}. \tag{16}$$

By construction, $E[\Delta(t)] = 0$ and $Var[\Delta(t)] = 1$ for any $0 < t < T$. Moreover, by the Central Limit Theorem, the distribution of $\Delta(t)$ approaches the standard Normal as N increases. This means, in particular, that a 95% confidence interval for the values of $\Delta(t)$ for any $0 < t < T$ is [–1.96, 1.96]. The test statistic is the maximal absolute deviation of the normalized bridge from zero, $X_B = \max|\Delta(t)|$. The quantiles of the test statistic (which are different from the quantiles of $\Delta(t)$ at any fixed t) are estimated by Monte-Carlo simulations. Although $\Delta(t)$ is asymptotically independent of T and N, we use simulations with the observed values of T and N, to minimize finite sample size effects.

5.1.2. The Kolmogorov-Smirnov Test

The Kolmogorov-Smirnov (KS) test is used to check if a sample comes from a specified distribution by comparing the empirical cumulative distribution function with the theoretical one. In a stationary Poisson process conditioned on the total number N of observed events, the event times t_i, $i = 1, \dots, N$, are i.i.d. random variables with the common uniform density on the observation interval $[\min(t_i) = t_{\min}, \max(t_i) = t_{\max}]$. Accordingly, the transformed times

$$u_i = \frac{t_i - t_{\min}}{t_{\max} - t_{\min}} \tag{17}$$

are i.i.d. uniform on [0,1]. The quantiles of the test statistic X_{KS}, which is the maximal deviation between the empirical and theoretical cumulative distribution functions, are computed by statistical software packages.

5.1.3. The Brown-Zhao (BZ) Test (Brown & Zhao, 2002)

This test is a ramification of the chi-square test. Specifically, we partition the observation time interval into K nonoverlapping segments of equal length and compute the number N_k, $k = 1, \dots, K$, of events within each segment. Define $Y_k = \sqrt{N_k + \frac{3}{8}}$ and $\overline{Y} = \frac{1}{K}\sum_{k=1}^{K} Y_k$. The test statistic is

$$\chi^2_{BZ} = 4\Sigma_{k=1}^{K}\left(Y_k - \overline{Y}\right)^2. \tag{18}$$

Under the stationary Poisson hypothesis, the test statistic is approximated by the chi-square distribution with K–1 degrees of freedom, which is used to compute the test p value.

The KS and BZ tests have been discussed by Luen and Stark (2012); we refer to this work for details of their performance.

5.2. Tests of Space-Time Independence

The tests and statistics considered in this section quantify deviations from a point field with independent space and time intensity components, allowing both time and space marginal distributions to be nonhomogeneous.

5.2.1. The Space-Time (ST) Factorization Test

We test the null hypothesis of independence of the time and space marginal components of the point field. Formally, the null assumes that the (conditional) intensity of the process allows space-time factorization:

$$H_0 : \Lambda(\mathbf{x}, t) = \Lambda_{\mathrm{space}}(\mathbf{x}) \times \Lambda_{\mathrm{time}}(t). \tag{19}$$

The test statistic X_{ST} is defined using the respective estimated intensities $\widehat{\Lambda}(\mathbf{x},t)$, $\widehat{\Lambda}_{\mathrm{space}}(\mathbf{x})$, and $\widehat{\Lambda}_{\mathrm{time}}(t)$:

$$R_{\mathrm{ST}}(\mathbf{x},t)=\frac{\widehat{\Lambda}(\mathbf{x},t)}{\widehat{\Lambda}_{\mathrm{space}}(\mathbf{x})\widehat{\Lambda}_{\mathrm{time}}(t)};X_{\mathrm{ST}}=\sup_{(\mathbf{x},t)}\{R_{\mathrm{ST}}(\mathbf{x},t)\}. \tag{20}$$

Informally, under the null hypothesis (19), the fraction R_{ST} is expected to assume values around unity. At the same time, clustering increases the values of the process intensity $\Lambda(\mathbf{x},t)$ with respect to the null expectation (19). This leads to increased values of R_{ST} (well above unity). Such increased values are traced by the test statistic X_{ST}. The significance of the test statistic is evaluated using the distribution of X_{ST} for reshuffled catalogs of the form $\{\mathbf{x}_i, t_{\pi(i)}\}$ for a significantly large collection of permutations π on $\{1, \dots, N\}$. The intensities can be estimated using different approaches (which of course can affect the test performance). In this work, we use a uniform density kernel smoothing, which means that the estimated density equals the proportion of events that occur within a spatiotemporal vicinity of an examined point. For instance, the space-time intensity is estimated as

$$\widehat{\Lambda}(\mathbf{x},t)=\frac{1}{N}\ \#\{(\mathbf{x}_i,t_i):r(\mathbf{x}_i,\mathbf{x})<r_0\ \text{ and }\ |t_i,t|<\tau_0\}. \tag{21}$$

Here $r(\mathbf{x},\mathbf{y})$ denotes the spatial distance between points $\mathbf{x}$ and $\mathbf{y}$; r_0 and τ_0 are the bandwidth parameters of the algorithm. The space and time marginal intensities are estimated in a similar fashion, using only spatial and temporal vicinity of an examined point, respectively. For computational efficiency, we only compute the value of the test statistic at the locations of catalog events: $\{\mathbf{x}_i,t_i\}$, $i=1,\dots,N$.

5.2.2. The Luen-Stark (LS) Test

This test, suggested by Luen and Stark (2012), is an adoption of a general test by Romano (1988, 1989) to the seismicity setting; we refer to these works for computational and methodological details. The test aims at checking if the times and space components of a process are independent. Formally, the test assesses the conditional exchangeability of event times given event locations, which is a weaker condition than independence (exchangeability follows from independence but not vice versa). The conditional exchangeability means that, given event locations, the distribution of event times $\{t_1, \dots, t_N\}$ is the same as the distribution of permuted times $\{t_{\pi(1)}, \dots, t_{\pi(N)}\}$ for any permutation π of $\{1, \dots, N\}$. We consider the empirical distribution P of the ST pairs $\{\mathbf{x},t\}$ that assigns probability N^{-1} to each pair $\{\mathbf{x}_i,t_i\}$, $i=1,\dots,N$; the permutation distribution P_π that assigns probability N^{-1} to each pair $\{\mathbf{x}_i,t_{\pi(i)}\}$, $i=1,\dots,N$ for a permutation π on $\{1,\dots,N\}$; and the independence distribution P_{ind} that assigns probability N^{-2} to each pair $\{\mathbf{x}_i,t_j\}$, $i,j=1,\dots,N$. The test statistic X_{LS} is defined as the maximal deviation between the independence and empirical distributions:

$$X_{\mathrm{LS}}(P)=\sup_V|P(V)-P_{\mathrm{ind}}(V)|, \tag{22}$$

where the maximum is taken over all lower-left quadrants of the form

$$V(\mathbf{x}_0,t_0)=\{(\mathbf{x},t)=(\varphi,\lambda,t):\varphi\le\varphi_0\ \text{ and }\ \lambda\le\lambda_0\ \text{ and }\ t\le t_0\}. \tag{23}$$

The significance of the test statistic is evaluated numerically using the distribution of X_{LS} (P_π) for a sufficiently large collection of permutations π on $\{1,\dots,N\}$. See Luen and Stark (2012) for further detail.

In the following sections we apply the declustering algorithm of section 4 and tests of section 5 to selected synthetic and real catalogs. Table 3 summarizes the values of used parameters and key information about the declustered catalogs.

6. Analysis of Epidemic Type Aftershock Sequence (ETAS) Model

The ETAS modeling framework introduced by Ogata (1988, 1999) is an efficient way to simulate earthquake flow (e.g., Field, 2007; Field et al., 2017; Harte, 2012; Helmstetter et al., 2006; Helmstetter & Sornette, 2002; Lippiello et al., 2014; Ogata, 2011). An ETAS model generates a marked point field by a self-exciting clustering mechanism. Specifically, background events occur according to a time-stationary space-inhomogeneous Poisson process with independent space and time components. Each background event generates offspring

Table 3
Parameters of Declustering Used in This Study and Selected Properties of Declustered Catalogs

Catalog	Epicentral dimension (d)	Proximity cutoff (η_0)	Cluster threshold (α_0)	Declustering results				
					Median p value[a]			
				p_{bg}	KS	BZ10	Bridge	LS
ETAS	1.6	10^{-1}	0	0.26 ± 0.003	0.52	0.55	0.75	0.43
World	1.3	10^{-1}	−0.6	0.22 ± 0.004	0.41	0.34	0.74	0.62
			0	0.43 ± 0.003	$<10^{-4}$	$<10^{-4}$	0.015	0.015
Southern California, $m \geq 2.5$	1.6	10^{-1}	−0.8	0.05 ± 0.002	0.05	0.02	0.21	0.3
			0	0.20 ± 0.002	$<10^{-4}$	$<10^{-4}$	0.005	$<10^{-4}$
Southern California, $m \geq 3.5$	1.6	10^{-1}	0	0.26 ± 0.006	0.47	0.83	0.49	0.05
Landers	1.6	10^{-1}	0	0.018 ± 0.001	10^{-4}	0.008	0.05	0.14
Parkfield	1.3	$10^{-2.5}$	−0.3	0.16 ± 0.005	0.15	0.002	0.23	0.18
			0	0.25 ± 0.005	$<10^{-4}$	$<10^{-4}$	0.03	0.15

Note. p_{bg} = average proportion of background events and respective 95% prediction interval (*not* error of the mean) in 10,000 independent realizations of declustering.
[a]According to 500 independent realizations of declustering, additional information about the distribution of p value is given in Figures 7, 9, 11, 13, 15, and 17.

(first generation events) according to a fixed ST kernel, these offspring generate their own offspring (second generation events) according to the same kernel and so on. The number of directly triggered events increases exponentially with event magnitude. The resulting seismic flow is a compound of background and triggered events from all generations. The main body of the work on ETAS operates under the assumption that the magnitudes of events (background and triggered) are independent and drawn from the Gutenberg-Richter (exponential) distribution (2) with a constant b value.

6.1. Examined Catalog

We work here with the ETAS catalog from Gu et al. (2013). The complete catalog spans a square spatial region of size 600 × 600 km and time interval of 8,000 days (21.9 years). We follow Gu et al. (2013) and remove the first 365 days from our analysis—this initial period is subject to simulation artifacts. The resulting catalog examined in this study includes 26,986 events, with 7,706 (28.5%) background events. The temporal history of the examined sequence of events is shown in Figure 3a. The catalog has 12 events with magnitude $m > 5.5$, each of which is associated with a clearly visible aftershock sequence. There are also other aftershock clusters related to smaller mainshocks. The space distribution of events in the original catalog is shown in Figure 4a. Figures 3a and 4a illustrate substantial variations of the event spatial intensity, with prominent increases around the locations of the largest events (marked by red circles). Figure 4b shows the space distribution of true background events; their geometry mimics that of the Southern California fault network. The information about the true background and triggered events available in the ETAS catalog allows us to perform a detailed assessment of declustering.

6.2. Initial Assessment of Declustering

A declustered catalog (a particular stochastic realization of thinning) that corresponds to $\alpha_0 = 0.1$ is illustrated in Figures 3b and 4c. We begin with a visual examination of the results. The space distribution of the estimated background events closely approximates the space distribution of the true background (cf. Figures 4b and 4c), with all major concentration areas, as well as low-intensity regions, being correctly identified. At the same time, some notable discrepancies are also present. One immediately visible deviation of the estimated background field from the true one is the existence of multiple estimated background events (Figure 4c) in the regions of low-to-zero intensity of the true background (Figure 4b). One such region, for instance, is located in the bottom left corner of the examined field ($x + y < 300$ km) in Figure 4b. This misidentification of triggered events as background is related to high spatiotemporal separation between the triggering events and some of their offspring in the ETAS model.

6.3. Stability of Declustering

Here we illustrate stability of declustering with respect to random realizations of the declustered catalog. The proposed declustering algorithm has a single "stiff" parameter—the cluster threshold α_0. The experiment of

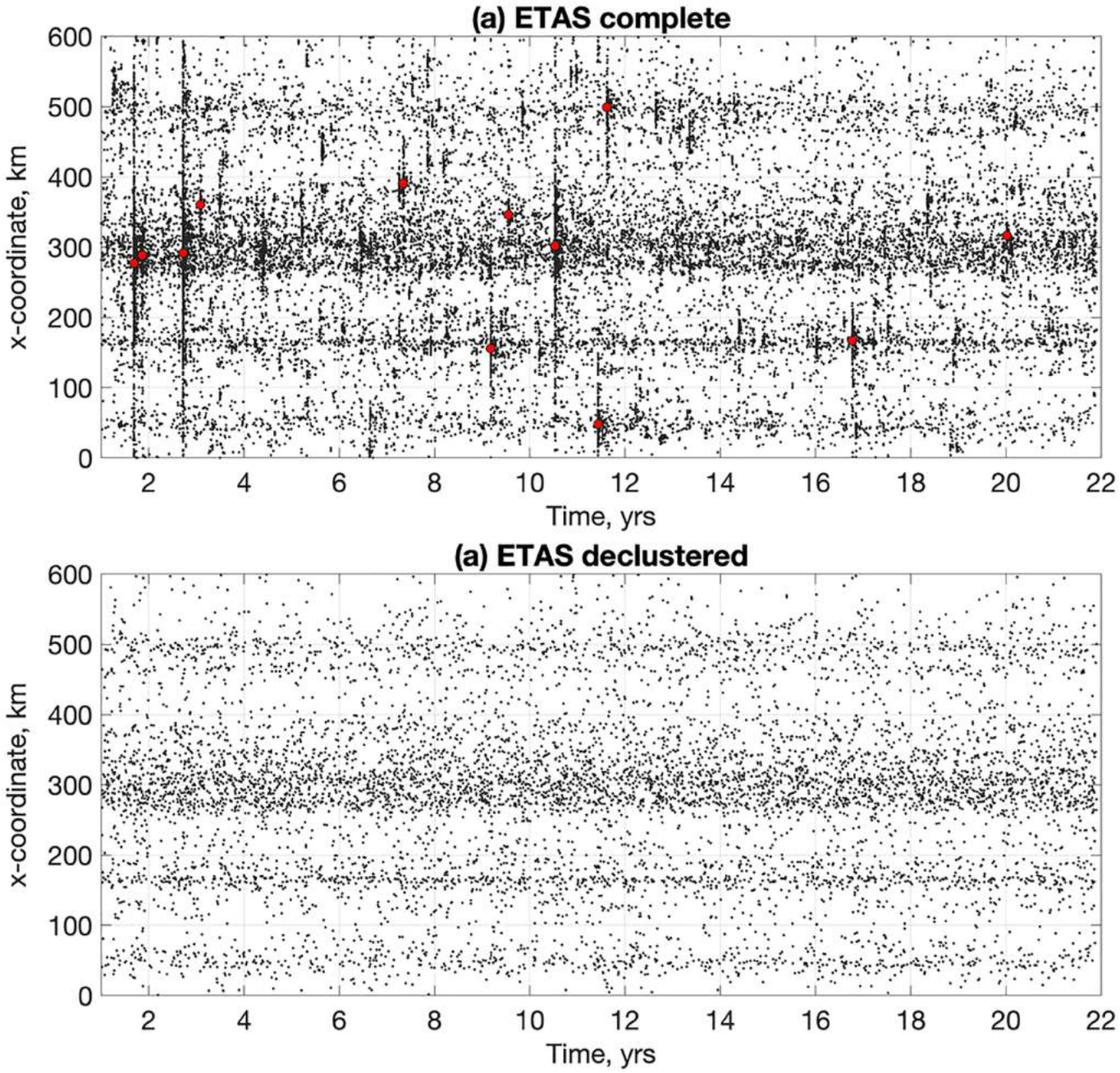

Figure 3. Declustering results for ETAS catalog of Gu et al. (2013). The x coordinate of events versus time. (a) Complete catalog, 26,986 events. The 12 largest events with $m > 5.5$ are shown by red circles. (b) Declustered catalog, a particular stochastic realization with $\alpha_0 = 0.1$. The declustered catalog consists of 7,771 events. The actual number of background events is 7,706.

this section uses 10,000 independent realizations of declustering at every examined value of the cluster threshold within the interval [–1, 1]. The other parameters are fixed at $d = 1.6$ and $\eta_0 = 10^{-1}$ (see Table 3).

Figure 5a shows the histogram of the empirical probabilities (proportions out of 10,000 trials) for a given event in the original catalog to be identified as a background event in declustering with cluster threshold $\alpha_0 = 1$. For example, if a selected event is identified as background in every realization out of 10,000, this empirical probability equals 1; if the event is always identified as clustered, it is equal

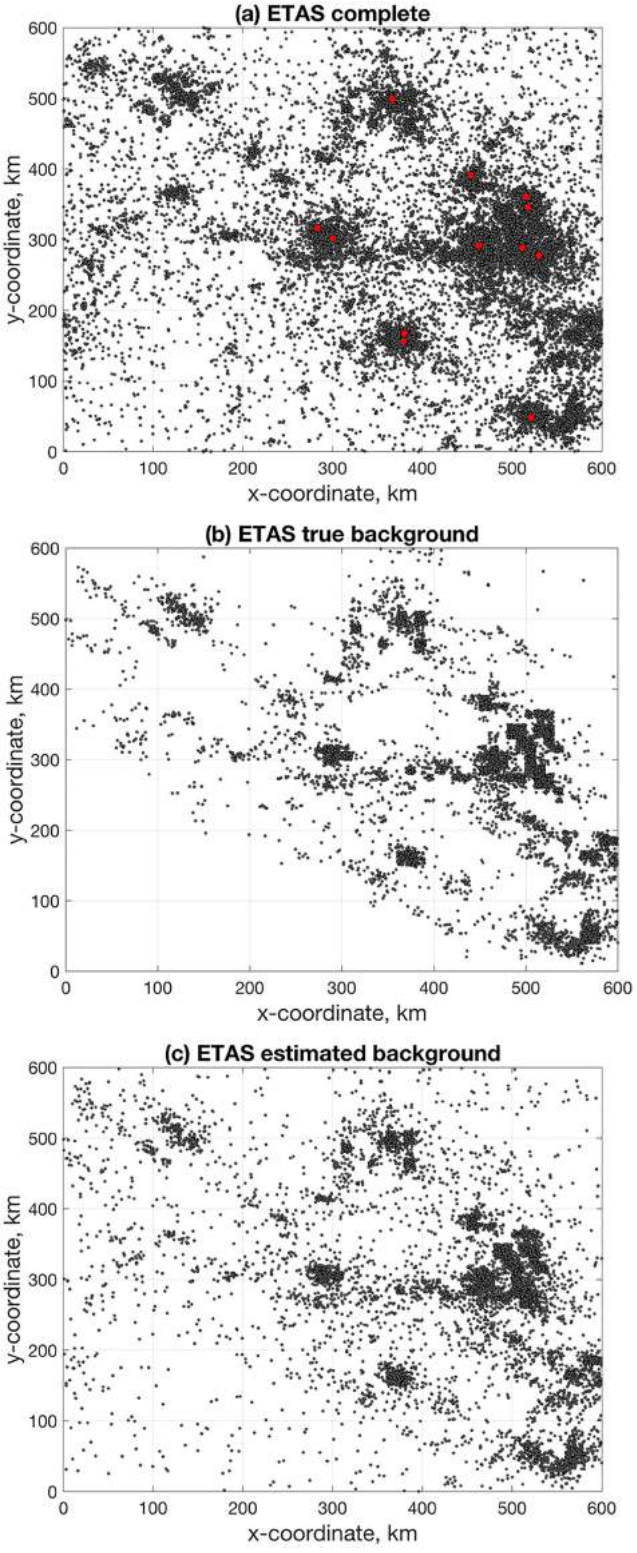

Figure 4. Declustering results for ETAS catalog of Gu et al. (2013). Spatial distribution of events. (a) Complete catalog, 26,986 events. The largest events with $m > 5.5$ are shown by red circles. (b) True background events, $N = 7{,}706$. (c) Declustered catalog, a particular stochastic realization with $\alpha_0 = 0.1$. The catalog consists of 7,771 events.

to 0; and so on. The histogram (blue bars) is prominently concentrated around the values 0 and 1, indicating that the majority of events are consistently identified either as background or cluster in most of the random realizations. The inset in panel (a) shows the proportion of events in the original catalog that have the same estimated type (background or cluster) in at least Q% of the random realizations (out of 10,000), as a function of cluster threshold α_0. This analysis confirms stability of event type identification: Over 65% (85%) of events in the original catalog have the same estimated type for *all* examined cluster thresholds in over 95% (75%) of random realizations.

Figure 5b shows the proportion of estimated background events (solid line) at different threshold values. The true proportion of 28.5% is depicted by the dashed horizontal line. The error bars show a 95% prediction interval for the estimated background proportions (*not* the error of the mean, which would be much narrower) observed in 10,000 independent realizations of random declustering at each value of α_0. This analysis shows that the estimated proportion (and hence the number) of background events is a very stable quantity for a given value of the cluster threshold. For instance, at $\alpha_0 = 0.1$, the stochastic variability of background proportion with respect to random realizations (measured as the width of the 95% prediction interval) amounts to 2% of the average value. This analysis also shows that the choice of threshold $\alpha_0 = 0.1$ used in section 6.2 corresponds to a close approximation of the true proportion of background events.

6.4. Quantitative Assessment of Declustering Quality

By definition of the ETAS model, its space and time marginal components are independent, and the time component of the true background field is a stationary Poisson process. Accordingly, if a declustering produces an estimated background field close enough to the true one, each of the tests discussed in section 5 should not reject its respective null hypothesis. We apply the BZ tests with $K = 10$ and $K = 100$ bins, which results in six tests total; this includes four tests in time domain (KS, BZ10, BZ100, and Bridge) and two space-time tests (LS and ST).

Figure 6 shows the test p values as a function of the threshold $-1 \le \alpha_0 \le 1$, for a single stochastic realization of the declustering at each α_0. Recall that the number of estimated background events increases with α_0 (see Figure 5b). In this experiment, we use the ST test with space bandwidth $r_0 = 100$ km and time bandwidth $\tau_0 = 3$ years. None of the six tests rejects the null (p values are above 0.05) for small thresholds $\alpha_0 \le 0.1$. For $\alpha_0 \ge 0.2$, the KS and both versions of the BZ tests reject the null (p values less than 0.05). The bridge test also shows a steady drop of its p values at $\alpha_0 \ge 0.2$, although it decreases under the level 0.05 (and hence formally rejects the null) only at $\alpha_0 \ge 0.4$. Both ST tests (LS and ST) do not reject the null until very high values of the threshold, $\alpha_0 \ge 0.9$. The results suggest that the estimated background field is not distinguishable from a stationary Poisson process for $\alpha_0 \le 0.1$ (at least, according to the tests used here). For larger values of the threshold, there appear significant temporal fluctuations, whose

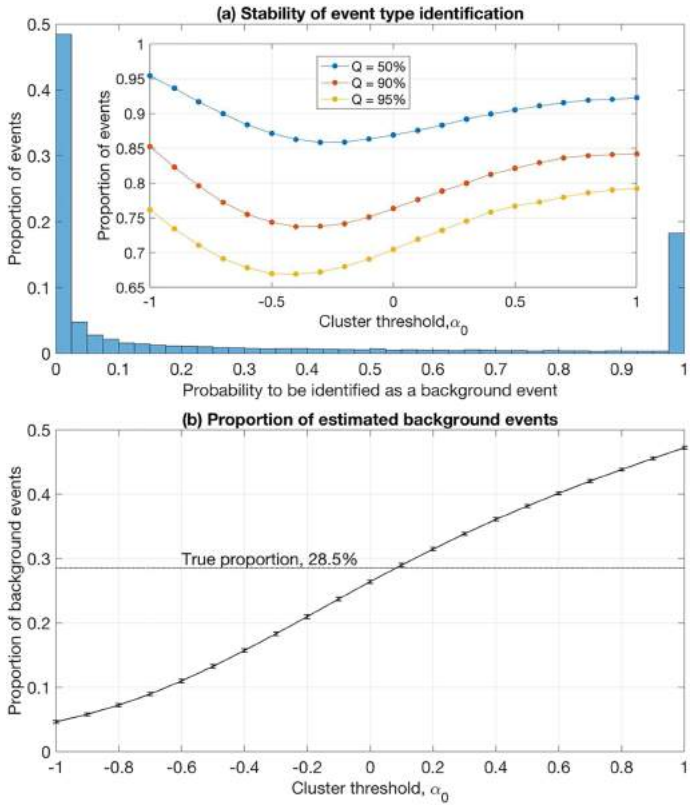

Figure 5. Declustering results for ETAS catalog of Gu et al. (2013). Stability of declustering. The analysis is done for 10,000 independent realizations of a declustered catalog for each value of cluster threshold α_0. (a) The main figure shows histogram of the empirical probability for a given earthquake to be identified as a background event (and hence included in the declustered catalog). The cluster threshold $\alpha_0 = 0.1$. The inset shows the proportion of events in the original catalog that have the same estimated type (background or triggered) in at least Q% of the declustering realizations out of 10,000, as a function of α_0. (b) The average (solid line) and 95% prediction interval (*not* the error of the mean) for the estimated proportion of background events as a function of the cluster threshold α_0. Dashed line shows the actual proportion (28.5%) of background events. The panel summarizes the results for 210,000 stochastic realizations of the declustered catalog.

magnitude increases with α_0 (this is suggested by the decreasing p values). At the same time, the estimated field has independent space and time marginal components even when its time component is nonstationary ($0.2 \le \alpha_0 \le 0.8$). Finally, for large values of the threshold ($\alpha_0 \ge 0.8$), the estimated background field is neither stationary in time nor it has independent space and time components. The transition from stationary to nonstationary behavior occurs at $\alpha_0 = 0.1$, which is the parameter value used in the analyses of section 6.2 (Figures 3 and 4). This value gives a very close match between the predicted and actual number of background events (Figure 5b). This might suggest a threshold selection strategy if one expects the background field to be stationary (or space-time independent): select the largest threshold value at which the set of examined tests, after using a suitable multiple test correction, does not rejects the null.

A more systematic analysis that considers stochastic variability of a declustered field is presented in Figure 7. Here we apply the tests discussed in section 5 to 500 independent stochastic realizations of declustering at each value of the cluster threshold α_0. The figure shows the empirical quantiles (2.5%, median, and 97.5%) of the resulting p values for selected tests. We notice that the results for a single declustering (Figure 6) closely match those for a large number of independent realizations (Figure 7). This indicates that the space-time patterns of declustered catalogs are stable and largely independent of a particular thinning realization, confirming the observations in section 6.3. The nominal quantiles in all examined cases deviate from the estimated ones, even when the null is not rejected. For example, the nominal median for the KS test in Figure 7a at small values of α_0 corresponds to p value of about 0.6; the same discrepancy is observed in other tests. This effect is expected. The estimated quantiles should (asymptotically) match the nominal ones if independent point fields are being tested (more specifically, if the test statistics calculated under the null hypothesis are independent). In our case, however, independent realizations of declustering do *not* result in independent point fields, since most estimated background events are the same in multiple stochastic realizations, as illustrated in section 6.3 (Figure 5).

The proportions of correct identifications are largely independent of the event magnitude. This is illustrated in Figure S1 that shows proportions of correctly identified events of different types in analysis of earthquakes with $m \ge m_{\min}$. In this experiment, the declustering is done 10,000 times at every value of $m_{\min}$ with $\alpha_0 = 0.1$ for the entire catalog. The proportions are computed then for different magnitude selections. The proportion of correctly identified triggered events (middle green line in Figure S1), with respect to the true triggered events, is almost constant and close to 87%. The proportion of correctly identified background events (bottom red line in Figure S1) with respect to the true background events is close to 70%. These proportions are stable and observed for all examined magnitude ranges. Despite imperfect identification of the true triggered and background events, the total number of estimated background events closely matches the true value (top blue line in Figure S1), which is consistent with Figure 5b. This happens because some true triggered events have been identified as background and replaced the $100\% - 70\% = 30\%$ of true background events incorrectly identified as triggered.

Table 4 summarizes the cross-classification of events of different types in 10,000 realizations of stochastic declustering. As before, we notice high stability of results with respect to the random realizations.

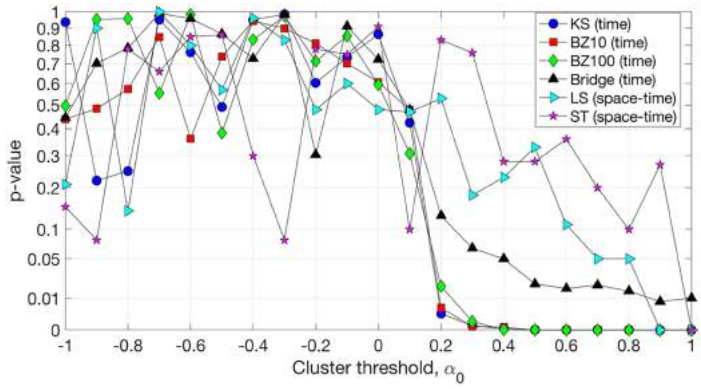

Figure 6. Declustering results for ETAS catalog of Gu et al. (2013). Testing hypothesis about stationarity and space-time independence of the estimated background field (see section 5). The test p values as a function of the cluster threshold α_0. The analysis uses a single stochastic realization of declustering for each value of α_0. The legend shows the abbreviated test names, as defined in section 5.

We also note the approximate equality (about 9%) of misclassifications of both types; this is a necessary condition for the total number of estimated background events to match the true number. The proportions in Table 2 do not match those in Figure S1; this is because Table 2 lists proportions with respect-to the total number of events in the catalog (the sum of all cells is 100%), while Figure S1 refers to proportions with respect to the total true number of events of a given type (triggered or background).

Figure S2 shows the proportion of correctly identified triggered (solid) and background (dashed) events depending on their proximity to the true parent or the nearest neighbor, respectively. The analysis refers to a single realization of stochastic declustering. For triggered events, the identification quality is almost perfect if event is close to its parent, $\log_{10}\eta < -2$. The identification quality deteriorates almost linearly with $\log_{10}\eta$, reaching the minimal value of 30% for $\log_{10}\eta = 5$. For background events, the identification quality is almost perfect if no event occurred closer than $\log_{10}\eta = 1$. The quality rapidly deteriorates for background events with closer nearest neighbors, because the existence of such close neighbors increases the probability for an event to be identified as triggered.

7. Analysis of Observed Seismicity

We now apply the declustering method of section 4 to selected observed catalogs. This illustrates the analysis in situations where we do not know the true event types (triggered vs. background) and cannot assume that the declustered field should be stationary. The descriptions of the examined data sets are given in section 2 and summarized in Table 1; the parameters and results of declustering are summarized in Table 3.

7.1. Global Seismicity

We analyze 22,694 earthquakes from the global NCEDC (2016) catalog during 2000–2015. Figures 8a and 8c show the map view and time-latitude sequence of the examined catalog, respectively. The catalog includes 19 earthquakes with $m \geq 8.0$. The minimal examined magnitude is $m_{\min} = 5$. This means that the catalog includes 19 sequences with at least three units of reported magnitudes below that of the mainshock. The Bath law (Båth, 1965; Shcherbakov & Turcotte, 2004; Vere-Jones, 1969) predicts that the largest aftershock magnitude is about one unit below the magnitude of the mainshock. Using this and the Gutenberg-Richter law for aftershocks with $b \approx 1$, we expect to have over 100 aftershocks for each of these large events. Moreover, the two largest earthquakes with $m \geq 9.0$ should have aftershocks sequences with at least 1,000 events each. Of course, smaller earthquakes also have their (generally smaller) aftershock sequences. The time-latitude sequence (Figure 8c) illustrates various forms of event clustering; this includes aftershock sequences, spatially varying earthquake intensity, and possible fluctuations of intensity and clustering at a fixed spatial location.

An example of a declustered catalog with $\alpha_0 = -0.5$ is shown in Figures 8b and 8d. This catalog contains 5,676 events, which is 25% of the original events. The declustered catalog preserves (at least coarsely) spatial fluctuations of the original earthquake field and removes obvious clusters that are visually apparent in Figure 8c.

Figure S3 illustrates high stability of the declustering results with respect to 10,000 random realizations of the algorithm at different values of the cluster threshold $-1 \leq \alpha_0 \leq 1$. For example, over 60% of events have the same estimated type in more than 90% of declustering realizations at any value of the threshold α_0. The proportions of estimated background events for a given value of cluster threshold α_0 are also very stable, with stochastic fluctuations of approximately 2% of the mean value. The number

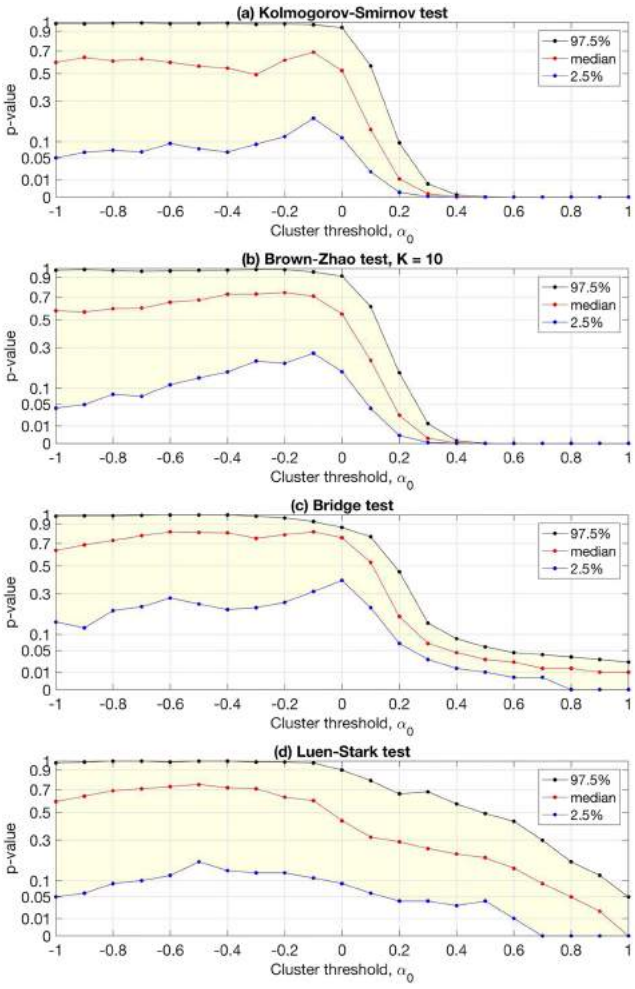

Figure 7. Declustering results for ETAS catalog of Gu et al. (2013). Testing hypothesis about stationarity and space-time independence of the estimated background field (see section 5). Empirical quantiles (97.5%, median, and 2.5%) for the distribution of p values obtained in 500 independent stochastic realizations of declustering at each value of α_0. Each panel summarizes the results of 10,500 individual tests. The y axis is rescaled to emphasize the behavior at low p values. (a) Kolmogorov-Smirnov test, (b) Brown-Zhao test with K=10, (c) Bridge test, (d) Luen-Stark test.

Table 4
Event Identification Quality in ETAS Catalog of Gu et al. (2013)

		True	
		Triggered	Background
Estimated	Triggered	62.5% ± 0.002%	8.7% ± 0.002%
	Background	8.9% ± 0.002%	19.8% ± 0.002%

Note. The results correspond to 10,000 realizations of stochastic declustering with $\alpha_0 = 0.1$. The margins of error indicate a 95% prediction interval (*not* error of the mean).

of estimated background events varies between 10% and 60% for cluster threshold α_0 increasing between −1 and 1.

Figure 9 summarizes the results of statistical testing for stationarity (panels a–c) and space-time independence (panel d) of declustered catalog. Both nulls cannot be rejected by any of the examined tests for small cluster thresholds $\alpha_0 < -0.5$, which correspond to less than 25% of estimated background events. Both nulls are rejected for larger threshold values that correspond to over 40% of estimated background events.

7.2. Southern California

The relocated catalog of seismicity in Southern California by Hauksson et al. (2012) is arguably the best regional earthquake catalog. It has unprecedented combination of quality of earthquake locations, spatiotemporal span, and range of reported magnitudes. We examine two versions of this catalog with different cutoff magnitudes.

The first analysis involves 43,633 events with $m \geq 2.5$. The original catalog (Figures 10a and 10c) shows multiple forms of clustering, including aftershock sequences (e.g., sequences of the largest events with $m \geq 7.0$ marked by red circles), swarm activity (e.g., a large swarm-type cluster at latitude $\phi \approx 33°$N during 1987–1990), and variations of seismic intensity at a given location (e.g., visible intensity gaps at latitudes $\phi > 36°$N during 2000–2006 and after 2015). Each of the three largest events in the catalog (see section 2 for details) with $m > 7.0$ is associated with a clearly visible aftershock sequence. Assuming the Bath and Gutenberg-Richter laws (as was done in section 7.1), one expects to have over 3,000 aftershocks in each sequence and over 10,000 aftershocks in the three sequences, which comprises over 20% of the examined events. A declustered catalog (Figures 10b and 10d) removes the aftershock and swarm clusters while preserving the overall spatial fluctuations of activity (e.g., seismicity at latitude $\phi \approx 34°$N is more intense than at latitude $\phi \approx 35°$N) and the abovementioned fluctuations of activity at specific locations. The stability analysis of declustering is illustrated in Figure S4.

The stationarity and space-time independence tests are summarized in Figure 11. As one might expect, the temporal variations of the original earthquake field not related to aftershocks or swarms (Figure 10c) should result in rejecting the stationarity null. This is confirmed by a formal analysis—all examined time tests reject the stationarity null for $\alpha_0 > -0.5$, which correspond to more than 10% of estimated background events. The space-time LS test rejects the space-time independence null for $\alpha_0 > -0.4$. This is different from what we observed in the analysis of ETAS data (Figures 6 and 7) and the global catalog (Figure 9), where the space-time tests were more liberal than the time tests. This observation is explained by varying intensity of estimated background events, most easily seen in the southmost (latitude $\phi <$ 32°N) and northmost (latitude $\phi >$ 35°N) regions of the declustered catalog (Figure 10d). A visual inspection of the original catalog (Figure 10c) suggests that these fluctuations are not declustering artifacts and are present also in the original catalog. Specifically, (i) a notable activity in the south in the original catalog only appears after 2010 (possibly being related to change of activity caused by the El Mayor-Cucapah earthquake and/or change in the network

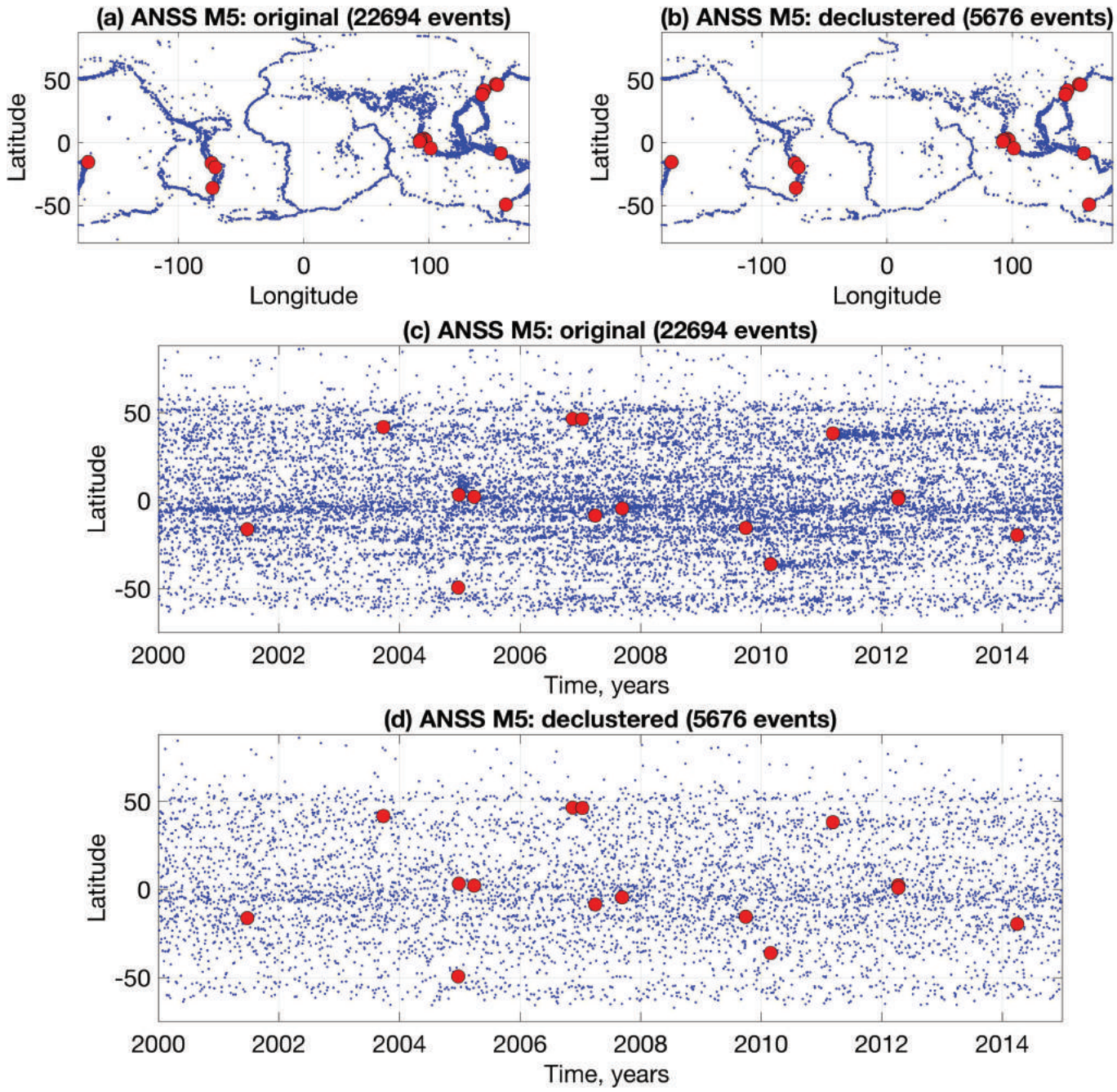

Figure 8. Declustering results in the global NCEDC catalog, $m \geq 5$. Cluster threshold $\alpha_0 = -0.5$. Red circle marks the earthquakes with $m > 8$. (a) Original catalog, map view. (b) Declustered catalog, map view. (c) Original catalog, time-latitude sequence. (d) Declustered catalog, time-latitude sequence.

configuration), and (ii) the regions of low intensity in the northern part of the declustered catalog (e.g., area with latitude $\phi > 35°$N during 2000–2006) correspond to low-intensity regions in the original catalog. These fluctuations of seismic intensity in selected regions might be not large enough to cause significant deviations in the temporal analysis (e.g., in KS test) but are readily seen in a space-time analysis (e.g., in LS test).

The second analysis in Southern California is done on 4,125 events with $m \geq 3.5$. This magnitude is arguably above the completeness threshold for the entire space-time domain of the catalog. The

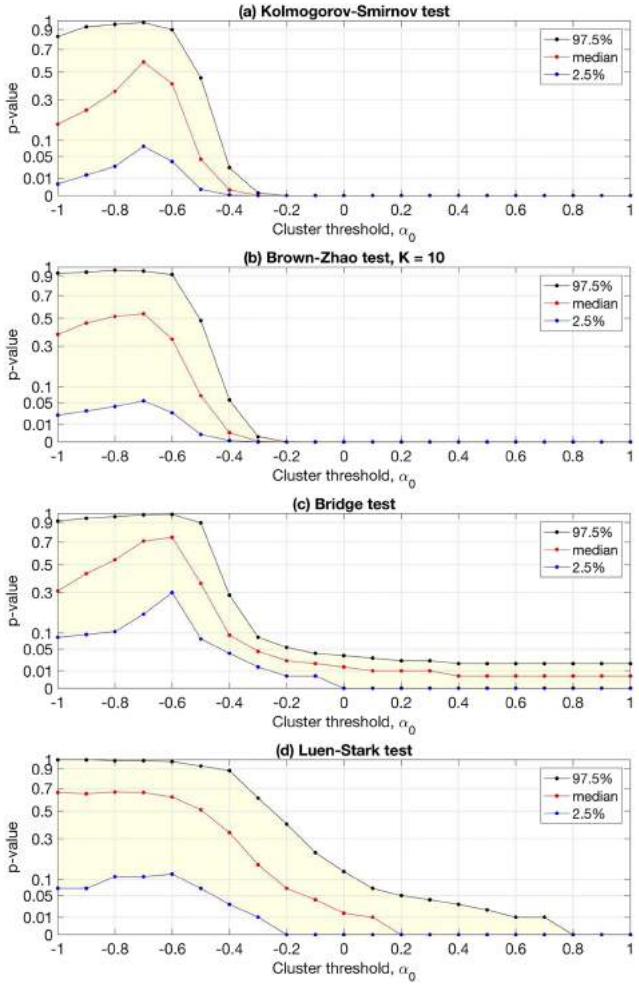

Figure 9. Declustering results in the global NCEDC catalog, $m \geq 5$. Testing hypothesis about stationarity and space-time independence of the estimated background field (see section 5). The analysis uses 500 independent realizations of declustering at each value of α_0. The rest of notations are the same as in Figure 7.

original catalog is illustrated in Figures 12a and 12c. A declustered version of the catalog with cluster threshold $\alpha_0 = 0.6$ (Figures 12b and 12d) does not include the most obvious aftershocks sequences (at least visually). The stationarity and space-time independence testing results are illustrated in Figure 13. Notably, each of examined time tests do not reject the stationarity null for most choices of cluster threshold ($-1 \leq \alpha_0 \leq 0.6$, which corresponds to 6–35% of background events); and the bridge test does not reject the null for all examined thresholds $-1 \leq \alpha_0 \leq 1$. At the same time, the LS time-space test rejects the null (e.g., the median p value falls below 0.05) already for $\alpha_0 > 0$, which corresponds to over 25% of background events. This effect has been discussed in the earlier analysis (Figure 11). The stability analysis is illustrated in Figure S5.

A declustered version of the Hauksson et al. (2012) catalog that contains 123,275 events with $m \geq 2.0$ is available in section S3. There we report the values of the normalized thresholds α_i, which allows one to obtain various versions of declustering.

7.3. Landers Rupture Zone

Here we examine seismicity around the rupture zone of the 1992 Landers earthquake—the largest event in the Southern California catalog of Hauksson et al. (2012). We consider earthquakes with $m \geq 0.0$, which is definitely below the completeness magnitude. This choice is intentional—we would like to examine the performance of the declustering algorithm in a situation of highly nonstationary background field, in a catalog heavily dominated by clustered events. The original catalog with 66,682 events (Figures 14a and 14c) shows a prominent change in space and time intensity of events associated with the occurrence of the Landers mainshock of 28 June 1992. The earthquake field before 1992 suggests that the natural background intensity is higher in the south part of the examined region. A declustered version of the catalog (Figures 14b and 14d) contains 1,671 events making only 2.5% of the original catalog. Importantly, the algorithm successfully removes the Landers aftershocks and does not produce space-time holes in the mainshock vicinity. The test results summarized in Figure 15 confirm the efficiency of the declustering algorithm in producing a quasi-stationary and approximately space-time independent field of background events even in this complicated situation. The stability analysis is illustrated in Figure S6.

7.4. Parkfield Region

Here we examine a subcatalog of Waldhauser and Schaff (2008) for Northern California around the Parkfield section of San Andreas fault. The original catalog with 8,648 events is illustrated in Figures 16a and 16c. The catalog has a single moderate earthquake—the Parkfield earthquake of 28 September 2004, $m = 6.0$, which produced a large aftershock sequence (Figure 16c). The intensity of events (events per year/km^2) in this catalog is much higher than in the other examples considered in this study. More specifically, the overall time intensity (0.94 events per day) is lower than in the other examined areas; however, the space concentration of earthquakes, which are confined within a very narrow fault zone, is very high. This is reflected in the distribution of the nearest-neighbor proximities, which is shifted toward lower values, and necessitates a cutoff proximity $\eta_0 = 10^{-2.5}$, which is lower than $\eta_0 = 10^{-1}$ that is used in our earlier examples. A declustered catalog is shown in Figures 16b and 16d, and the testing results are shown in Figure 17. Interestingly, the space-time independence is not rejected for the entire range of the cluster threshold values $-1 \leq \alpha_0 \leq 1$ examined

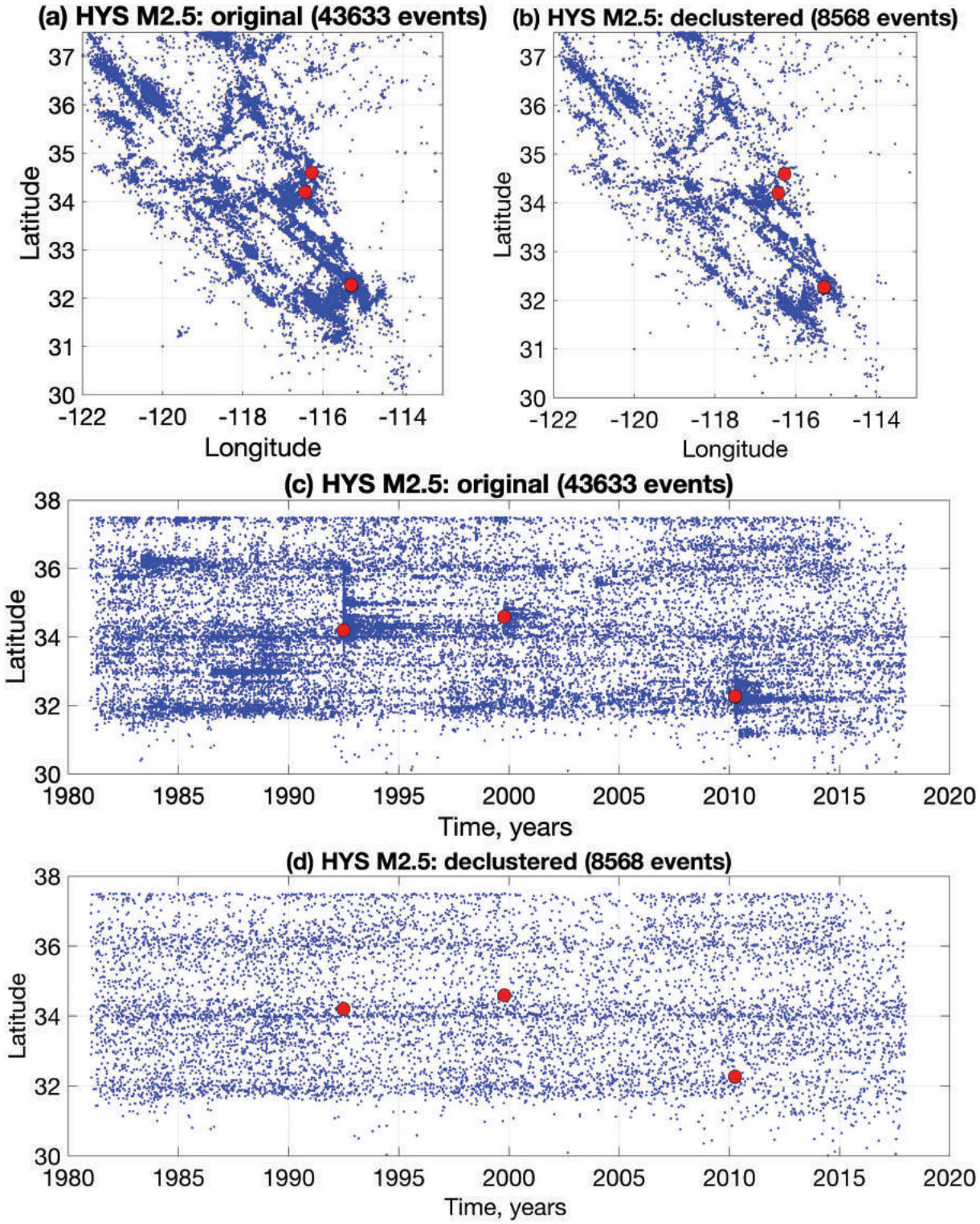

Figure 10. Declustering results for Southern California, $m \geq 2.5$, catalog of Hauksson et al. (2012). Cluster threshold $\alpha_0 = 0$. Red circle marks the earthquakes with $m \geq 7$. (a) Original catalog, map view. (b) Declustered catalog, map view. (c) Original catalog, time-latitude sequence. (d) Declustered catalog, time-latitude sequence.

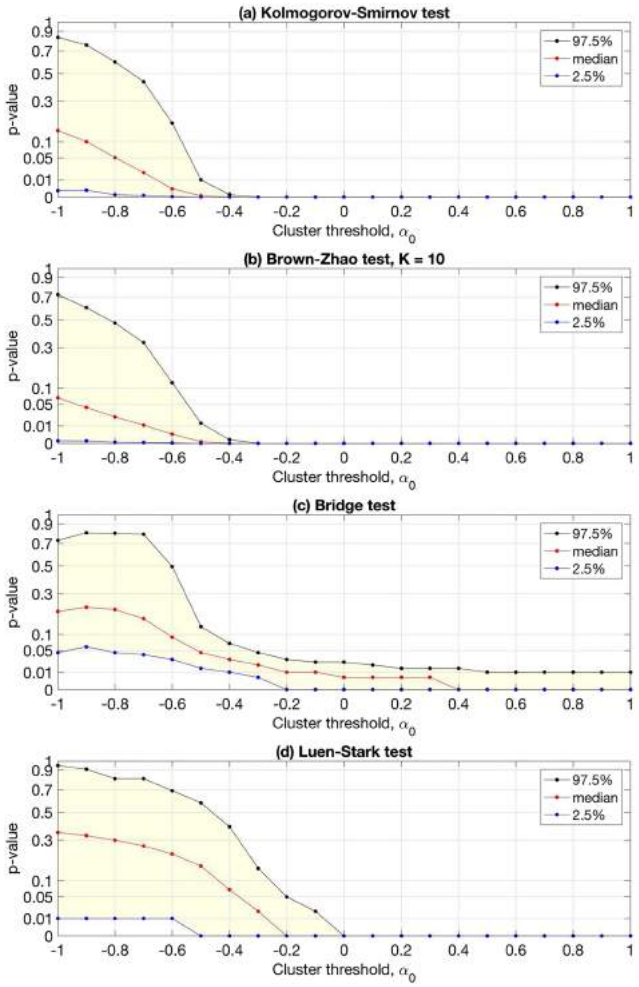

Figure 11. Declustering results for Southern California, $m \geq 2.5$, catalog of Hauksson et al. (2012). Testing hypothesis about stationarity and space-time independence of the estimated background field (see section 5). The analysis uses 500 independent realizations of declustering at each value of α_0. The rest of notations are the same as in Figure 7.

here (Figure 17d). The rejection of the time stationarity at relatively small values of α_0 by the KS and BZ tests (Figure 17b) is related to the increase of intensity of low-magnitude events ($m < 1.5$) after 2002. This increase can be readily detected by plotting the cumulative number of events as a function of time; it might reflect preparation processes that led to the Parkfield mainshock or be an artifact of event registration. In the context of this study, we emphasize that this increase is a property of the original catalog and not an artifact of the declustering procedure. The stability analysis is illustrated in Figure S7.

8. Discussion

This study develops an approach to earthquake catalog declustering based on nearest-neighbor analysis of seismicity in space-time-magnitude domain. The nearest-neighbor analysis has been used so far to detect and classify different types of earthquake clusters and examine statistical properties of the clusters in relation to physical properties of the lithosphere and anthropogenic forcing (see section 1). The problem of declustering, albeit closely related to the problem of cluster identification, has different success metrics and requires additional efforts. The main challenge is related to substantial overlap of the space-time domains of aftershocks and background. To statistically reconstruct background events that would have occurred within the aftershock sequences (and other cluster forms), we use (i) a magnitude-independent version of the proximity (1) and (ii) a space-dependent thinning of most clustered events (Steps 3 and 4 in section 4.1).

Our approach aims at simplicity and flexibility of practical use. In short, we quantify the degree of clustering of each earthquake i by a scalar quantity—the normalized nearest-neighbor proximity α_i of equation (7), and remove clustered events using a random thinning calibrated by the cluster threshold α_0. The algorithm requires a rough estimation of fractal dimension d of epicenters and an initial cutoff proximity value η_0 to evaluate relative intensity of background events in different areas. The algorithm is robust with respect to these two parameters. The cutoff proximity η_0 often can be readily estimated from the bimodal distribution of the nearest-neighbor proximities $\{\eta_i\}$ (see Figure S8). The declustered catalog is most sensitive to the cluster threshold α_0, which directly controls the number of background events. Importantly, in all examined data sets, the algorithm is able to produce a stationary declustered field with independent space and time components for sufficiently low values of α_0 (sufficiently low number of background events). Both the stationarity and space-time independence are being rejected as α_0 increases (at different values of α_0 for different catalogs). It is up to the user to decide how severe a deviation from the null can be tolerated in each specific application. From a computational point of view, producing alternative realizations of declustering for different values of α_0 is a very fast procedure that does not require reevaluation of the normalized nearest-neighbor proximities α_i. Oftentimes, selection of a proper threshold α_0 can be facilitated by bimodality of the empirical distribution of the normalized proximities $\{\alpha_i\}$, although this property is not required.

The problem of earthquake declustering does not have a rigorous mathematical definition, since we know neither the ground truth about the cluster conditional intensity nor the actual classification of events into background and clustered (other than in synthetic cases). More elementally, we do not even know if natural seismicity actually operates in these terms (background, clustered, etc.). At present, declustering efforts are guided by expert opinion, practical needs, and methods developed in relation

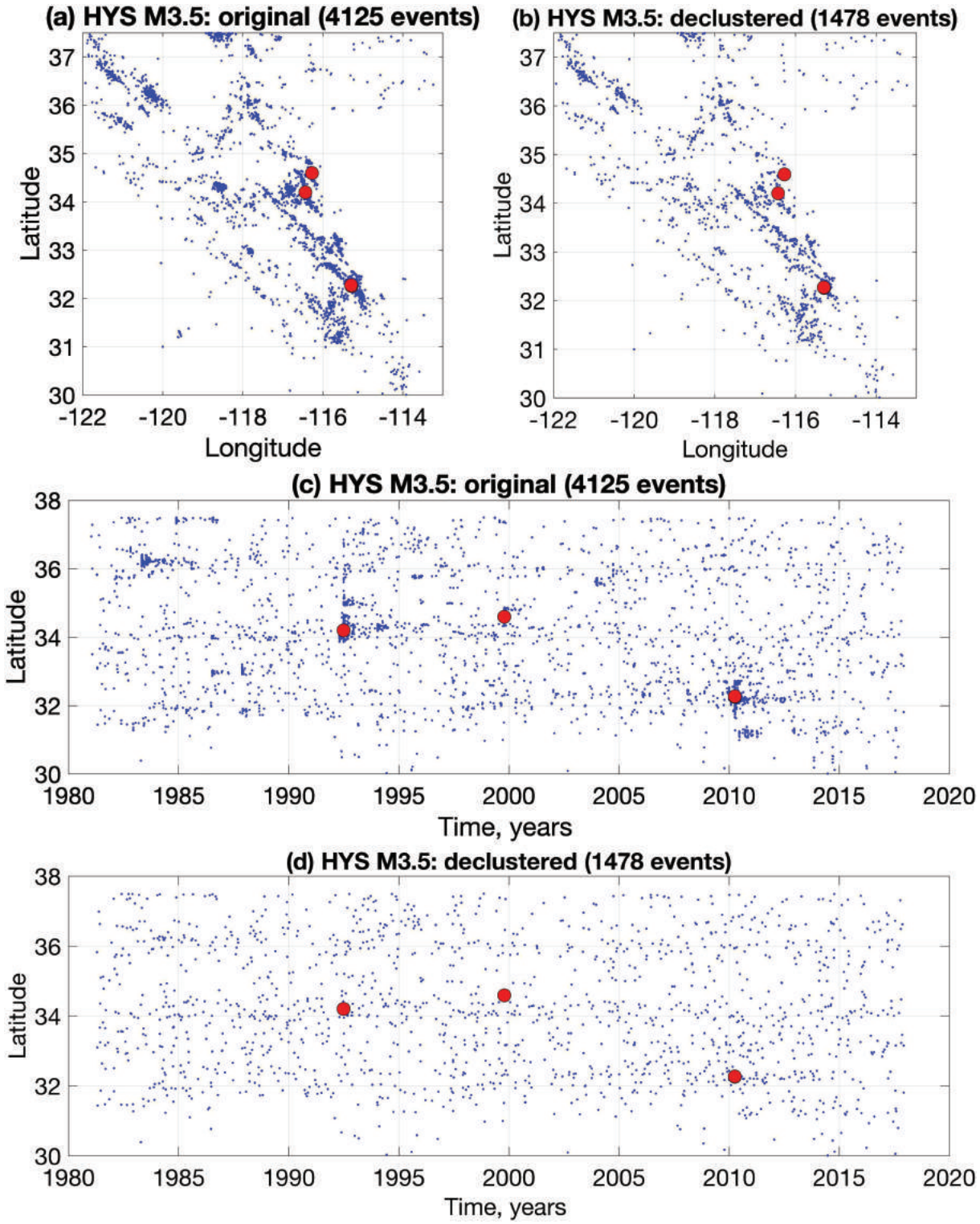

Figure 12. Declustering results for Southern California, $m \geq 3.5$, catalog of Hauksson et al. (2012). Cluster threshold $\alpha_0 = 0.6$. Red circle marks the earthquakes with $m \geq 7$. (a) Original catalog, map view. (b) Declustered catalog, map view. (c) Original catalog, time-latitude sequence. (d) Declustered catalog, time-latitude sequence.

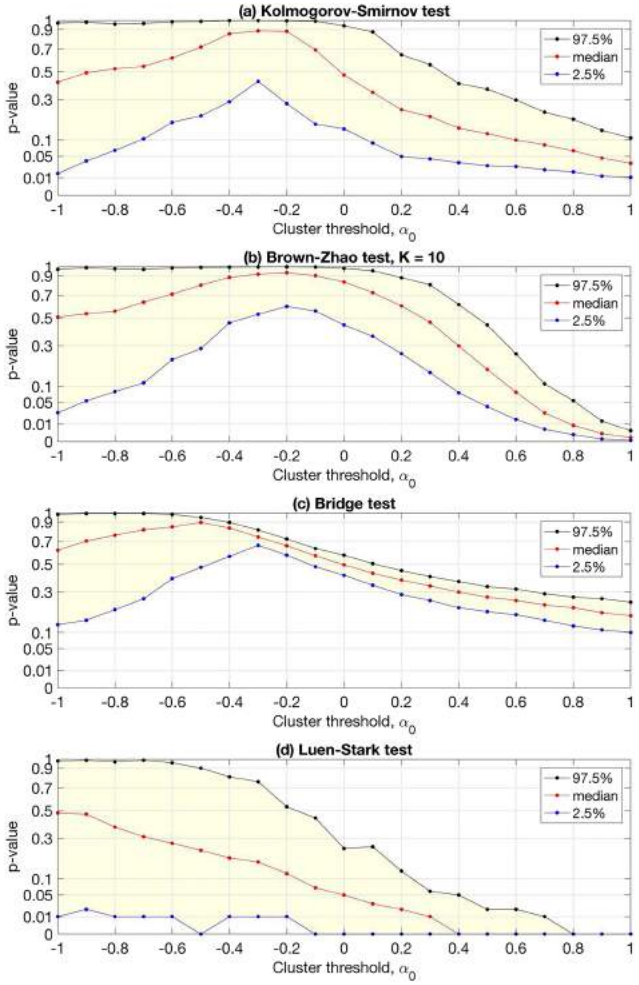

Figure 13. Declustering results for Southern California, $m \geq 3.5$, catalog of Hauksson et al. (2012). Testing hypothesis about stationarity and space-time independence of the estimated background field (see section 5). The analysis uses 500 independent realizations of declustering at each value of α_0. The rest of notations are the same as in Figure 7.

to particular cluster models. Accordingly, we do not attempt to develop a method with a unique suggested answer. Instead, the proposed technique allows the user to control the number of background events in the declustered catalog (via the cluster threshold α_0) while ensuring stability of the relative background intensities at different locations and filling artificial holes in the vicinity of the mainshocks. A practical "stopping criterion" can be easily formulated based on the total number of background events (e.g., "retain 25% of the catalog") or test results (e.g., "keep the maximal number of background events for which the Poisson null is not rejected"). Such criteria, however, should depend on the catalog and practical problem at hand; no general rule seems to be available at the moment. We believe that the proposed adaptive approach is the best match to the current, incomplete, understanding of earthquake clustering.

Informally, the goal of declustering is understood as identifying "background" events that would have occurred in the absence of triggering by other events. Gardner and Knopoff (1974) suggested that one might think of a catalog as a mixture of two populations—"*aftershock clusters which are not Poissonian, and main sequence events which may or may not be*" (their p. 1363). Indeed, the aftershock sequences are responsible for the most notable fluctuations of seismicity rates, which may increase several orders of magnitude after a large earthquake (e.g., Figure 1), depending on the range of magnitudes reported in a catalog. Under this two-population mixture assumption, the problem of declustering is reduced to identifying and removing aftershocks—events triggered by other events. Gardner and Knopoff (1974) examined several catalogs in Southern California with magnitude cutoffs m_c between 3.8 and 5.3 using a window declustering approach and found that the resulting catalogs cannot be distinguished from a stationary Poisson sequence by a chi-square test. This gave an impetus to the perception that a properly declustered catalog is Poissonian in time. A later important study by Reasenberg (1985) that used the second-moment properties of the earthquake field has found that a declustered catalog with $m_c = 4.0$ in Southern California is also Poissonian (yet possibly nonhomogeneous) in space. This has established the commonly accepted null model for declustered seismicity—a Poisson point field that is stationary in time and inhomogeneous in space.

The recently available high-quality relocated catalogs (e.g., Hauksson et al., 2012; Waldhauser & Schaff, 2008) allow performing declustering analysis with a much higher range of magnitudes than those considered by Gardner and Knopoff (1974) or Reasenberg (1985). Such analyses reveal multiple forms of clustering complementary to mainshock-aftershock sequences. This notably includes foreshocks, swarms, and fluctuations of seismic activity at a given location caused by various forcing (e.g., postseismic motion below the seismogenic crust, tidal, seasonal, climatic, and anthropogenic). The increasing observational evidence cast a doubt on the Poissonian character of a declustered field and suggest reconsidering the declustering quality metrics (e.g., Luen & Stark, 2012).

The proposed declustering approach has no assumptions about the expected form of earthquake clusters (e.g., a Poisson cluster model and Omori-type clusters) or resulting declustered field (e.g., a stationary Poisson point process). This being said, the algorithm successfully reconstructs stationary and space-time independent background field assumed in a synthetic ETAS catalog (section 6 and Figures 6 and

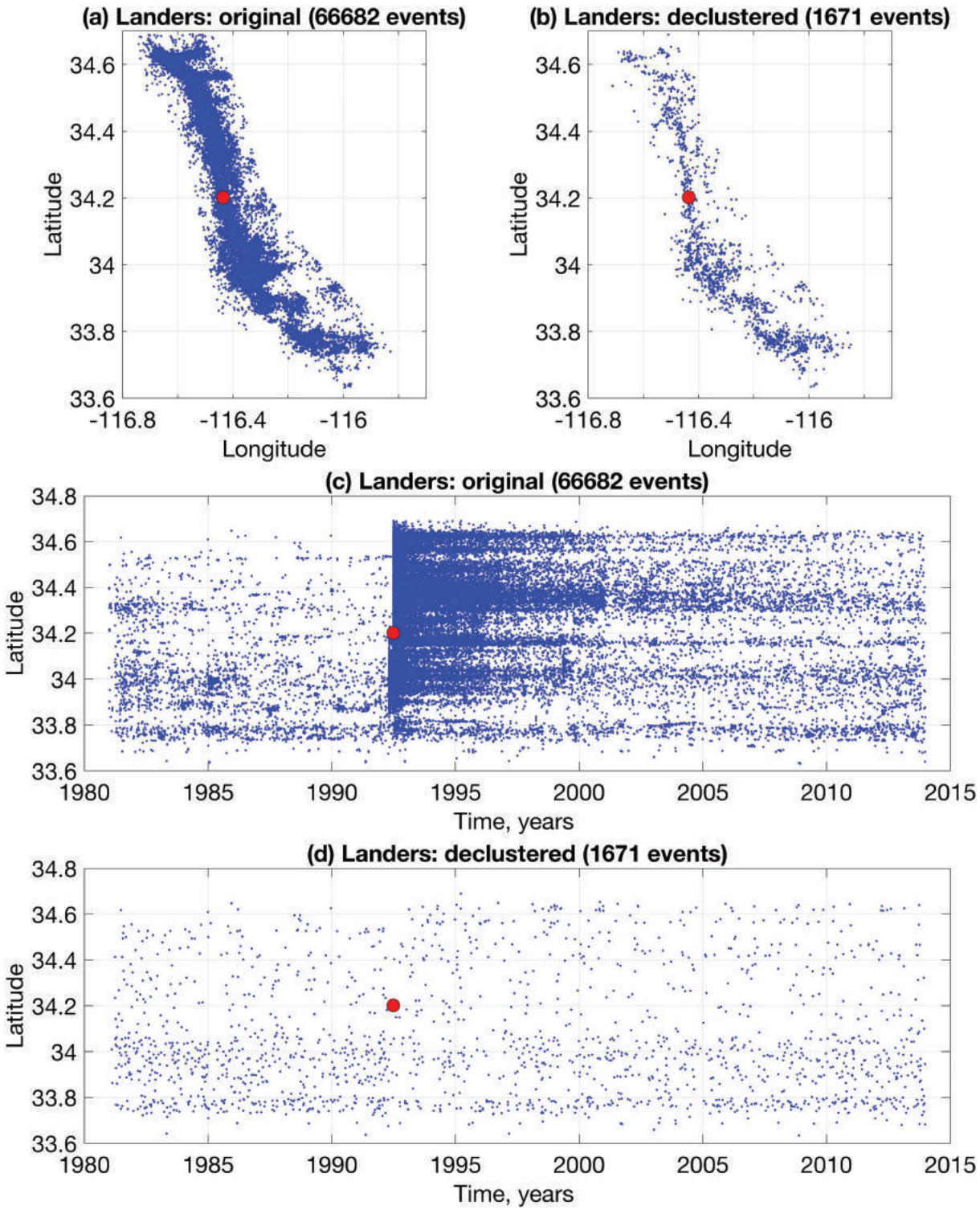

Figure 14. Declustering results for Landers (1992, M7.3) subcatalog of Hauksson et al. (2012). Cluster threshold $\alpha_0 = 0.2$. Red circle marks the Landers earthquake, 1992, M7.3. (a) Original catalog, map view. (b) Declustered catalog, map view. (c) Original catalog, time-latitude sequence. (d) Declustered catalog, time-latitude sequence.

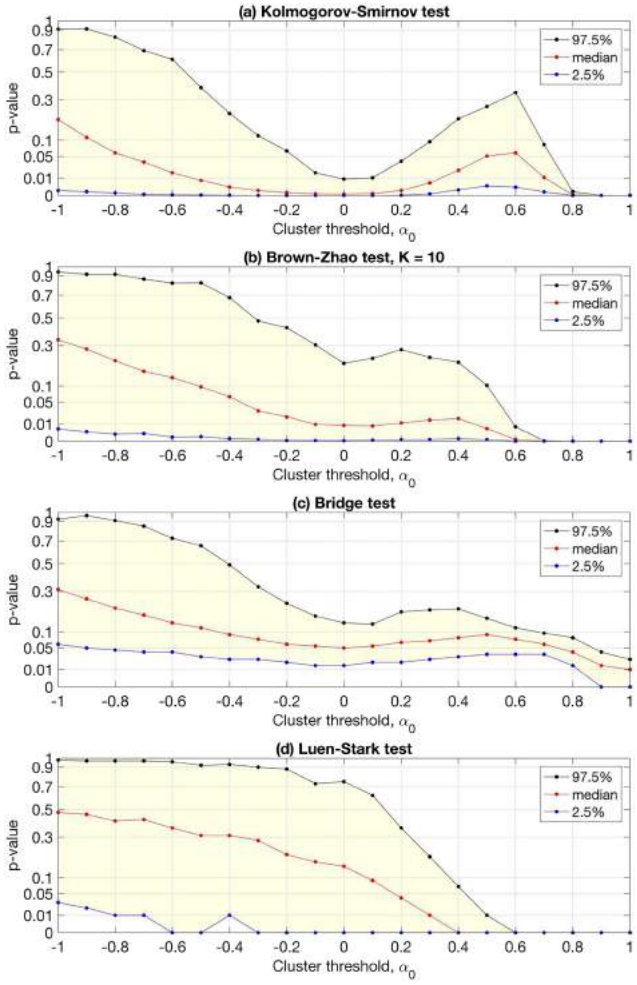

Figure 15. Declustering results for Landers (1992, M7.3) subcatalog of Hauksson et al. (2012). Testing hypothesis about stationarity and space-time independence of the estimated background field (see section 5). The analysis uses 500 independent realizations of declustering at each value of α_0. The rest of notations as in Figure 7.

7), with the majority of events being correctly identified as background or clustered (Table 4). The algorithm aims at preserving the generic space-time features of the original catalog —geometry of fault network and relative long-term rates of background events (Figure 4). In the global analysis (section 7.1), the estimated background is stationary and space-time independent for up to 25% of events being recognized as background (Figure 9). In the analysis of Southern California with a cutoff magnitude $m_c = 3.5$ (section 7.2), the estimated background is stationary for up to 35% of events being recognized as background (Figures 13a–13c); the background is also space-time independent for up to 25% of events recognized as background (Figure 13d). These numbers are consistent with earlier works in Southern California and support the classical hypothesis about stationary and ST independent background in catalogs with small-to-intermediate range of magnitudes ($\Delta m = m_{max} - m_{min} < 4$). However, in the Southern California catalog with $m_c = 2.5$ ($\Delta m = m_{max} - m_{min} = 4.8$), the algorithm only produces a stationary background when keeping less than 5% of events as background (Figure 11), which is much less than conventional estimations of the background proportions (~25–30%). In analysis with 25–30% of events left in the background, the field is clearly nonstationary, and its time and space components are dependent (Figure 11). These deviations from stationarity and space-time independence can be easily traced back to the original set of earthquakes; they seem to be intrinsic features of the recorded earthquake flow (which reflects the actual physical processes and reporting issues) that should be preserved in the background field (section 7.2 and Figure 10). We expect similar properties of recorded data in other seismogenic regions.

Similar to the nearest-neighbor cluster detection analysis, the proposed declustering algorithm is robust with respect to catalog location uncertainties and magnitude incompleteness. However, one should be careful when examining catalogs with varying location errors and completeness levels, which create changes in the background intensity. The spatial extent of the minimum event used in the nearest-neighbor analysis should be larger than the location error, and spatiotemporal variations in the location errors and magnitude of completeness can produce, if not accounted for, corresponding apparent spatial variations of background seismicity rate (Zaliapin & Ben-Zion, 2015). Similarly, increased earthquake rates during the intervals of decreased completeness magnitude may be confused with clustering and hence lead to biased results.

The algorithm can be modified in several ways. In some situations, it might be justified to use space-dependent initial cutoff proximity η_0. Earlier regional and global analyses (Zaliapin & Ben-Zion, 2013b, 2016a) indicate that the nearest-neighbor proximity threshold (computed with $w = 1$) that separates clustered and background populations varies in space. The nearest-neighbor proximities for different values of w (including $w = 0$) should preserve this space-dependent variation of background-versus-cluster threshold. These threshold variations, however, are mainly caused by the space-dependent proximities within the background mode (reciprocally related to the space-dependent background intensity), while the clustered proximities remain approximately constant. This may reflect approximate similarity of aftershock triggering process in different environments. Our analysis shows that using a space-independent cutoff proximity η_0 may work well for regional or global analysis with small-to-intermediate range of examined magnitudes, $\Delta m = m_{max} - m_{min} < 4$. Calculating a space-varying

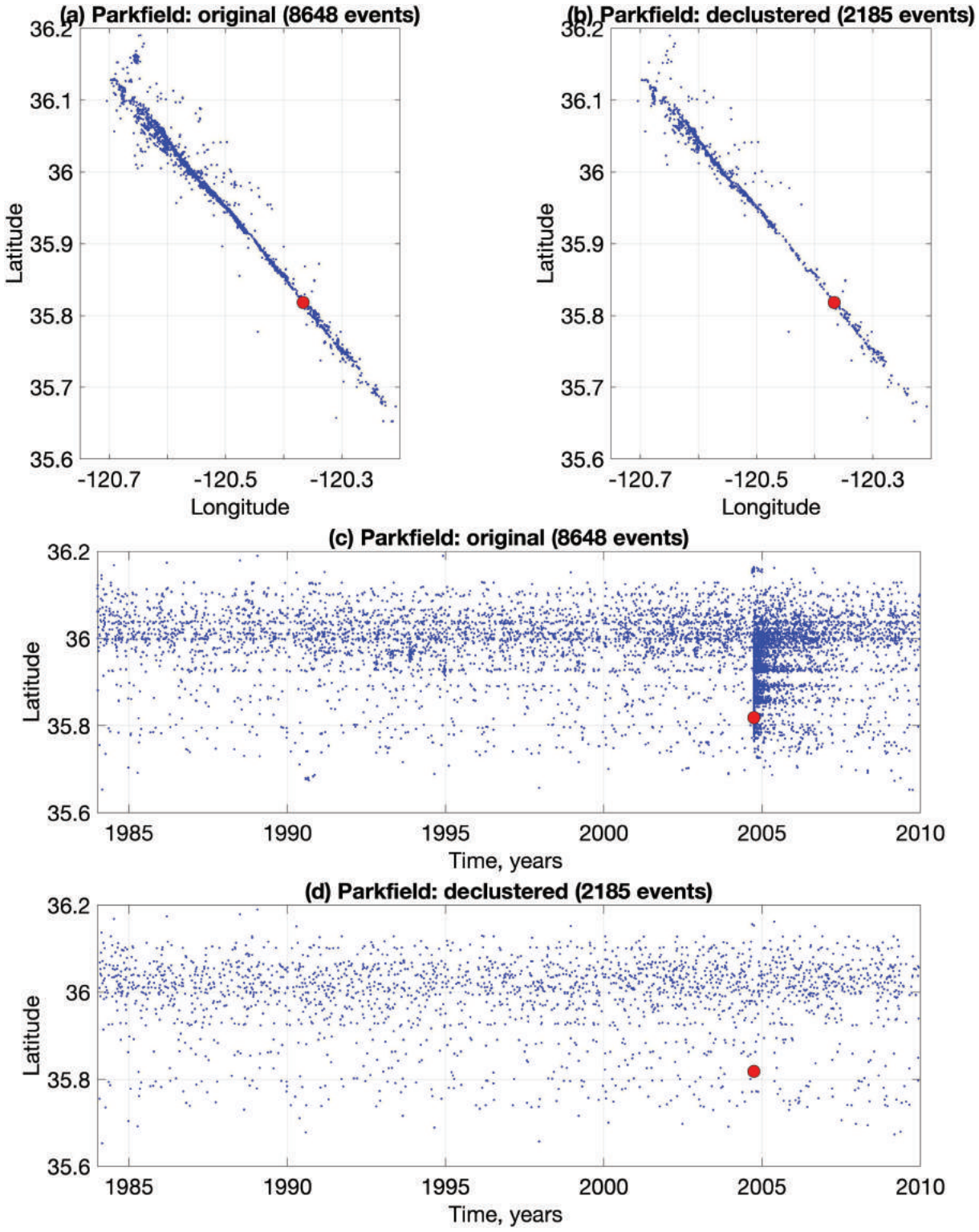

Figure 16. Declustering results for Parkfield (2004, M6) subcatalog of Waldhauser and Schaff (2008). Cluster threshold $\alpha_0 = 0.0$. Red circle marks the Parkfield earthquake, 2004, M6.0. (a) Original catalog, map view. (b) Declustered catalog, map view. (c) Original catalog, time-latitude sequence. (d) Declustered catalog, time-latitude sequence.

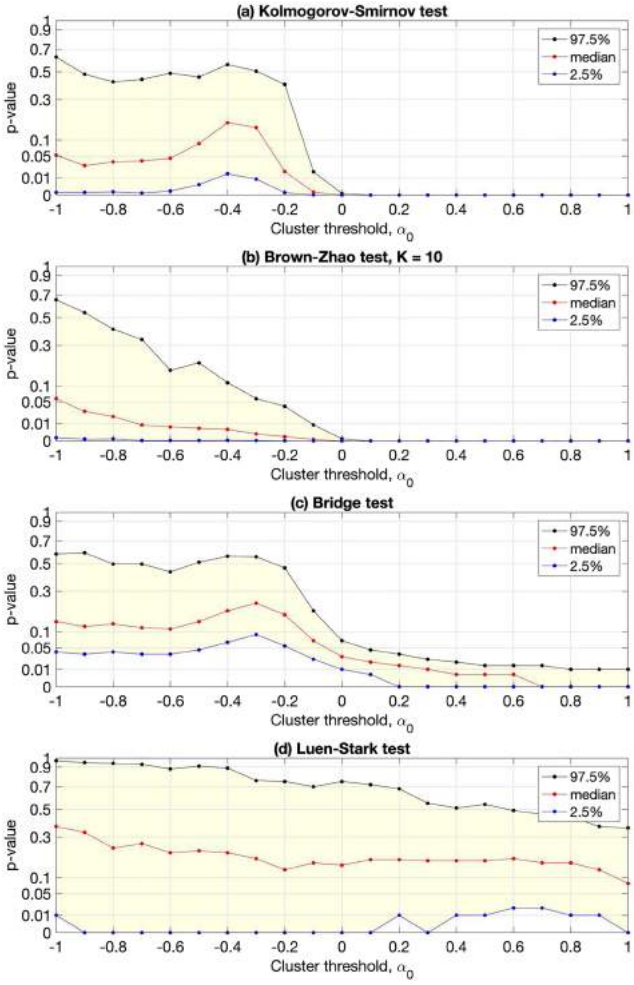

Figure 17. Declustering results for Parkfield (2004, M6) subcatalog of Waldhauser and Schaff (2008). Testing hypothesis about stationarity and space-time independence of the estimated background field (see section 5). The analysis uses 500 independent realizations of declustering at each value of α_0. The rest of notations as in Figure 7.

threshold complicates the algorithm parameterization (due to multiple decisions and parameters related to space-dependent analysis) and increases the processing time. Using a space-dependent estimation may be justified if the examined catalog includes areas with substantially different seismic intensities, for instance, if one examines a Northern California catalog including the Geysers field or a Central California catalog including the Long Valley caldera region. In general, we recommend examining cases with significantly different background intensities (order of magnitude difference) separately.

Another possible modification is related to a more elaborate thinning procedure. In particular, the functional dependence of $P_{\mathrm{back},i}$ on α_i, currently given by equation (8), can be selected in relation to a specific hypothesis about the nearest-neighbor proximity of clustered and/or background events. We provide a background on the distributional properties of the nearest-neighbor proximity in section S1.

The stationary time in the randomized-reshuffled catalogs may be replaced with a kernel smoothing of the events that satisfy $\eta_i > \eta_0$. This is justified if one expects the background intensity to change in time, for example, in volcanic areas or in catalogs with changing completeness level. Furthermore, in cases of a very good separation between the background and cluster modes (reflected in the well-separated modes of the proximity distribution, see Figure S8), one can replace synthetic times with reshuffling of the observed times independent of the reshuffling of event locations.

It is possible to implement an iterative declustering procedure that stops, for example, when the distribution of the normalized nearest-neighbor proximities α_i does not significantly deviate from a Weibull distribution (which indicates absence of clustering). The idea of iterative declustering has been used by Marsan and Lengline (2008) in a different statistical framework.

At this stage, it is hard to tell if the increase in complexity related the abovementioned (and other possible) modifications is justified by a related increase in declustering quality. This will be explored in future studies.

Acknowledgments

We are grateful to two anonymous reviewers and anonymous Associate Editor for useful comments. The research was supported by the National Science Foundation (Grants EAR-1723033 and EAR-1722561), the Earthquake Hazards Program of the USGS (Grants G17AP00086 and G17AP00087), and the Southern California Earthquake Center (based on NSF Cooperative Agreement EAR-1600087 and USGS Cooperative Agreement G17 AC00047). The global NCEDC (2019) catalog is available online (http://www.quake.geo.berkeley.edu/anss/). The Southern California catalog of Hauksson et al. (2019) is available online (http://scedc.caltech.edu/research-tools/downloads.html).

References

Abolfathian, N., Martínez-Garzón, P., & Ben-Zion, Y. (2019). Spatiotemporal variations of stress and strain parameters in the San Jacinto fault zone. *Pure and Applied Geophysics*, *176*(3), 1145–1168. https://doi.org/10.1007/s00024-018-2055-y

Baiesi, M., & Paczuski, M. (2004). Scale-free networks of earthquakes and aftershocks. *Physical Review E*, *69*, 066106. https://doi.org/10.1103/PhysRevE.69.066106

Båth, M. (1965). Lateral inhomogeneities in the upper mantle. *Tectonophysics*, *2*(6), 483–514. https://doi.org/10.1016/0040-1951(65)90003-X

Ben-Zion, Y. (2008). Collective behavior of earthquakes and faults: Continuum-discrete transitions, evolutionary changes and corresponding dynamic regimes. *Reviews of Geophysics*, *46*, RG4006. https://doi.org/10.1029/2008RG000260

Ben-Zion, Y., & Lyakhovsky, V. (2006). Analysis of aftershocks in a lithospheric model with seismogenic zone governed by damage rheology. *Geophysical Journal International*, *165*(1), 197–210.

Ben-Zion, Y., Rice, J. R., & Dmowska, R. (1993). Interaction of the San Andreas fault creeping segment with adjacent great rupture zones, and earthquake recurrence at Parkfield. *Journal of Geophysical Research*, *98*(B2), 2135–2144. https://doi.org/10.1029/92JB02154

Brown, L. D., & Zhao, L. H. (2002). A test for the Poisson distribution. *Sankhy: The Indian Journal of Statistics, Series A*, 611–625.

Clements, R. A., Schoenberg, F. P., & Veen, A. (2012). Evaluation of space–time point process models using super-thinning. *Environmetrics*, *23*(7), 606–616. https://doi.org/10.1002/env.2168

Cochran, E. S., Vidale, J. E., & Tanaka, S. (2004). Earth tides can trigger shallow thrust fault earthquakes. *Science*, *306*(5699), 1164–1166. https://doi.org/10.1126/science.1103961

Daley, D. J., & Vere-Jones, D. (2003). *An introduction to the theory of point processes. Volume I: Elementary theory and methods*. New York: Springer Science & Business Media, 2nd edn.

The Northern California catalog of Waldhauser and Schaff (2019) is available online (https://www.ldeo.columbia.edu/~felixw/NCAeqDD/). The ETAS catalog of Gu et al. (2019) is available in Supporting Information section of that paper (https://agupubs.onlinelibrary.wiley.com/doi/full/10.1002/jgrb.50306).

Daley, D. J., & Vere-Jones, D. (2008). *An introduction to the theory of point processes. Volume II: General theory and structure*. New York: Springer Science & Business Media, 2nd edn.

Davidsen, J., Kwiatek, G., Charalampidou, E. M., Goebel, T., Stanchits, S., Rück, M., & Dresen, G. (2017). Triggering processes in rock fracture. *Physical Review Letters*, *119*, 068501. https://doi.org/10.1103/PhysRevLett.119.068501

Davis, S. D., & Frohlich, C. (1991). Single-link cluster analysis, synthetic earthquake catalogues, and aftershock identification. *Geophysical Journal International*, *104*(2), 289–306. https://doi.org/10.1111/j.1365-246X.1991.tb02512.x

Ellsworth, W. L. (2013). Injection-induced earthquakes. *Science*, *341*, 1225942. https://doi.org/10.1126/science.1225942

Ellsworth, W. L. (2019). From foreshocks to mainshocks: Mechanisms and implications for earthquake nucleation and rupture propagation. *Mechanics of Earthquake Faulting*, *202*, 95–112. https://doi.org/10.3254/978-1-61499-979-9-95

Fialko, Y., Simons, M., & Agnew, D. (2001). The complete (3-D) surface displacement field in the epicentral area of the 1999 Mw7. 1 Hector Mine earthquake, California, from space geodetic observations. *Geophysical Research Letters*, *28*(16), 3063–3066. https://doi.org/10.1029/2001GL013174

Field, E. H. (2007). Overview of the working group for the development of regional earthquake likelihood models (RELM). *Seismological Research Letters*, *78*(1), 7–16. https://doi.org/10.1785/gssrl.78.1.7

Field, E. H., Milner, K. R., Hardebeck, J. L., Page, M. T., van der Elst, N., Jordan, T. H., et al. (2017). A spatiotemporal clustering model for the Third Uniform California Earthquake Rupture Forecast (UCERF3-ETAS): Toward an operational earthquake forecast. *Bulletin of the Seismological Society of America*, *107*(3), 1049–1081. https://doi.org/10.1785/0120160173

Fujii, Y., Satake, K., Sakai, S. I., Shinohara, M., & Kanazawa, T. (2011). Tsunami source of the 2011 off the Pacific coast of Tohoku Earthquake. *Earth, Planets and Space*, *63*(7), 815–820. https://doi.org/10.5047/eps.2011.06.010

Gao, S. S., Silver, P. G., Linde, A. T., & Sacks, I. S. (2000). Annual modulation of triggered seismicity following the 1992 Landers earthquake in California. *Nature*, *406*(6795), 500–504.

Gardner, J. K., & Knopoff, L. (1974). Is the sequence of earthquakes in Southern California, with aftershocks removed, Poissonian? *Bulletin of the Seismological Society of America*, *64*(5), 1363–1367.

Gentili, S., Di Giovambattista, R., & Peresan, A. (2017). Seismic quiescence preceding the 2016 central Italy earthquakes. *Physics of the Earth and Planetary Interiors*, *272*, 27–33. https://doi.org/10.1016/j.pepi.2017.09.004

Gentili, S., Peresan, A., Talebi, M., Zare, M., & Di Giovambattista, R. (2019). A seismic quiescence before the 2017 Mw 7.3 Sarpol Zahab (Iran) earthquake: Detection and analysis by improved RTL method. *Physics of the Earth and Planetary Interiors*, *290*, 10–19. https://doi.org/10.1016/j.pepi.2019.02.010

Goebel, T. H. W., & Brodsky, E. E. (2018). The spatial footprint of injection wells in a global compilation of induced earthquake sequences. *Science*, *361*(6405), 899–904. https://doi.org/10.1126/science.aat5449

Goebel, T. H. W., Rosson, Z., Brodsky, E. E., & Walter, J. I. (2019). Aftershock deficiency of induced earthquake sequences during rapid mitigation efforts in Oklahoma. *Earth and Planetary Science Letters*, *522*, 135–143. https://doi.org/10.1016/j.epsl.2019.06.036

Gu, C., Schumann, A. Y., Baiesi, M., & Davidsen, J. (2013). Triggering cascades and statistical properties of aftershocks. *Journal of Geophysical Research: Solid Earth*, *118*, 4278–4295. https://doi.org/10.1002/jgrb.50306

Hainzl, S. (2004). Seismicity patterns of earthquake swarms due to fluid intrusion and stress triggering. *Geophysical Journal International*, *159*(3), 1090–1096. https://doi.org/10.1111/j.1365-246X.2004.02463.x

Hainzl, S., Scherbaum, F., & Beauval, C. (2006). Estimating background activity based on interevent-time distribution. *Bulletin of the Seismological Society of America*, *96*(1), 313–320. https://doi.org/10.1785/0120050053

Hammond, W. C., Kreemer, C., Zaliapin, I., & Blewitt, G. (2019). Drought-triggered magmatic inflation, crustal strain and seismicity near the Long Valley Caldera, Central Walker Lane. *Journal of Geophysical Research: Solid Earth*, *124*, 6072–6091. https://doi.org/10.1029/2019JB017354

Harte, D. S. (2012). Bias in fitting the ETAS model: A case study based on New Zealand seismicity. *Geophysical Journal International*, *192*(1), 390–412.

Hauksson, E., Stock, J., Hutton, K., Yang, W., Vidal-Villegas, J. A., & Kanamori, H. (2011). The 2010 Mw 7.2 El Mayor-Cucapah Earthquake Sequence, Baja California, Mexico and Southernmost California, USA: Active seismotectonics along the Mexican Pacific Margin. *Pure and Applied Geophysics*, *168*(8-9), 1255–1277. https://doi.org/10.1007/s00024-010-0209-7

Hauksson, E., Yang, W., & Shearer, P. M. (2012). Waveform relocated earthquake catalog for Southern California (1981 to June 2011). *Bulletin of the Seismological Society of America*, *102*(5), 2239–2244. https://doi.org/10.1785/0120120010

Helmstetter, A., Kagan, Y. Y., & Jackson, D. D. (2006). Comparison of short-term and time-independent earthquake forecast models for Southern California. *Bulletin of the Seismological Society of America*, *96*(1), 90–106. https://doi.org/10.1785/0120050067

Helmstetter, A., & Sornette, D. (2002). Subcritical and supercritical regimes in epidemic models of earthquake aftershocks. *Journal of Geophysical Research*, *107*(B10), 2237. https://doi.org/10.1029/2001JB001580

Hill, D. P. (1977). A model for earthquake swarms. *Journal of Geophysical Research*, *82*(8), 1347–1352. https://doi.org/10.1029/JB082i008p01347

Hill, D. P., Reasenberg, P. A., Michael, A., Arabaz, W. J., Beroza, G., Brumbaugh, D., et al. (1993). Seismicity remotely triggered by the magnitude 7.3 Landers, California, earthquake. *Science*, *260*(5114), 1617–1623. https://doi.org/10.1126/science.260.5114.1617

Johnson, C. W., Fu, Y., & Bürgmann, R. (2017). Stress models of the annual hydrospheric, atmospheric, thermal, and tidal loading cycles on California faults: Perturbation of background stress and changes in seismicity. *Journal of Geophysical Research: Solid Earth*, *122*, 10,605–10,625. https://doi.org/10.1002/2017JB014778

Johnson, C. W., Fu, Y., & Bürgmann, R. (2019). Hydrospheric modulation of stress and seismicity on shallow faults in southern Alaska. *Earth and Planetary Science Letters*, *530*, 115904. https://doi.org/10.1016/j.epsl.2019.115904

Jones, L. M. (1985). Foreshocks and time-dependent earthquake hazard assessment in Southern California. *Bulletin of the Seismological Society of America*, *75*(6), 1669–1679.

King G. C. P., & Cocco, M. (2001). Fault interaction by elastic stress changes: New clues from earthquake sequences. *Advances in Geophysics*. Academic Press, 44, 1–38. https://doi.org/10.1016/S0065-2687(00)80006-0

Kisslinger, C. (1996). Aftershocks and fault-zone properties. *Advances in Geophysics*, *38*, 1–36. https://doi.org/10.1016/S0065-2687(08)60019-9

Kossobokov, V. G., & Nekrasova, A. K. (2017). Characterizing aftershock sequences of the recent strong earthquakes in Central Italy. *Pure and Applied Geophysics*, *174*(10), 3713–3723. https://doi.org/10.1007/s00024-017-1624-9

Langbein, J., Borcherdt, R., Dreger, D., Fletcher, J., Hardebeck, J. L., Hellweg, M., et al. (2005). Preliminary report on the 28 September 2004, M 6.0 Parkfield, California earthquake. *Seismological Research Letters*, *76*(1), 10–26. https://doi.org/10.1785/gssrl.76.1.10

Lay, T., Kanamori, H., Ammon, C. J., Nettles, M., Ward, S. N., Aster, R. C., et al. (2005). The great Sumatra-Andaman earthquake of 26 december 2004. *Science*, *308*(5725), 1127–1133. https://doi.org/10.1126/science.1112250

Lippiello, E., Giacco, F., Arcangelis, L. D., Marzocchi, W., & Godano, C. (2014). Parameter estimation in the ETAS Model: Approximations and novel methods. *Bulletin of the Seismological Society of America*, *104*(2), 985–994. https://doi.org/10.1785/0120130148

Lohman, R. B., & McGuire, J. J. (2007). Earthquake swarms driven by aseismic creep in the Salton Trough, California. *Journal of Geophysical Research*, *112*, B04405. https://doi.org/10.1029/2006JB004596

Luen, B., & Stark, P. B. (2012). Poisson tests of declustered catalogues. *Geophysical Journal International*, *189*(1), 691–700. https://doi.org/10.1111/j.1365-246X.2012.05400.x

Marsan, D., & Lengline, O. (2008). Extending earthquakes' reach through cascading. *Science*, *319*(5866), 1076–1079. https://doi.org/10.1126/science.1148783

Martínez-Garzón, P., Ben-Zion, Y., Abolfathian, N., Kwiatek, G., & Bohnhoff, M. (2016). A refined methodology for stress inversions of earthquake focal mechanisms. *Journal of Geophysical Research: Solid Earth*, *121*, 8666–8687. https://doi.org/10.1002/2016JB013493

Martínez-Garzón, P., Zaliapin, I., Ben-Zion, Y., Kwiatek, G., & Bohnhoff, M. (2018). Comparative study of earthquake clustering in relation to hydraulic activities at geothermal fields in California. *Journal of Geophysical Research*, *123*(5), 4041–4062. https://doi.org/10.1029/2017JB014972

McGuire, J. J. (2019). The geology of earthquake swarms. *Nature Geoscience*, *12*(2), 82–83. https://doi.org/10.1038/s41561-019-0302-1

Mignan, A. (2014). The debate on the prognostic value of earthquake foreshocks: A meta-analysis. *Scientific Reports*, *4*, 4099. https://doi.org/10.1038/srep04099

Molchan, G., & Dmitrieva, O. (1992). Aftershock identification: Methods and new approaches. *Geophysical Journal International*, *109*(3), 501–516. https://doi.org/10.1111/j.1365-246X.1992.tb00113.x

Møller, J., & Schoenberg, F. P. (2010). Thinning spatial point processes into Poisson processes. *Advances in Applied Probability*, *42*(2), 347–358. https://doi.org/10.1239/aap/1275055232

Moradpour, J., Hainzl, S., & Davidsen, J. (2014). Nontrivial decay of aftershock density with distance in Southern California. *Journal of Geophysical Research: Solid Earth*, *119*, 5518–5535. https://doi.org/10.1002/2014JB010940

NCEDC (2016) Northern California Earthquake Data Center. UC Berkeley Seismological Laboratory. Dataset. https://doi.org/10.7932/NCEDC

Ogata, Y. (1988). Statistical models for earthquake occurrences and residual analysis for point processes. *Journal of the American Statistical Association*, *83*(401), 9–27. https://doi.org/10.1080/01621459.1988.10478560

Ogata, Y. (1999). Seismicity analysis through point-process modeling: A review. In *Seismicity patterns, their statistical significance and physical meaning*, (pp. 471–507). Switzerland: Birkhäuser, Basel.

Ogata, Y. (2011). Significant improvements of the space-time ETAS model for forecasting of accurate baseline seismicity. *Earth, Planets and Space*, *63*(3), 217–229.

Ogata, Y., Utsu, T., & Katsura, K. (1995). Statistical features of foreshocks in comparison with other earthquake clusters. *Geophysical Journal International*, *121*(1), 233–254. https://doi.org/10.1111/j.1365-246X.1995.tb03524.x

Omori, F. (1894). On the aftershocks of earthquakes. *Journal of the College of Science, Imperial University of Tokyo.*, *7*, 111–200.

Peresan, A., & Gentili, S. (2018). Seismic clusters analysis in Northeastern Italy by the nearest-neighbor approach. *Physics of the Earth and Planetary Interiors*, *274*, 87–104. https://doi.org/10.1016/j.pepi.2017.11.007

Petersen, M. D., Moschetti, M. P., Powers, P. M., Mueller, C. S., Haller, K. M., Frankel, A. D., et al. (2015). The 2014 United States national seismic hazard model. *Earthquake Spectra*, *31*(1_suppl), S1–S30. https://doi.org/10.1193/120814EQS210M

Petersen, M. D., Mueller, C. S., Moschetti, M. P., Hoover, S. M., Rukstales, K. S., McNamara, D. E., et al. (2018). 2018 One-year seismic hazard forecast for the Central and Eastern United States from induced and natural earthquakes. *Seismological Research Letters*, *89*(3), 1049–1061. https://doi.org/10.1785/0220180005

Reasenberg, P. (1985). Second-order moment of central California seismicity, 1969–1982. *Journal of Geophysical Research*, *90*(B7), 5479–5495. https://doi.org/10.1029/JB090iB07p05479

Reverso, T., Marsan, D., & Helmstetter, A. (2015). Detection and characterization of transient forcing episodes affecting earthquake activity in the Aleutian Arc system. *Earth and Planetary Science Letters*, *412*, 25–34. https://doi.org/10.1016/j.epsl.2014.12.012

Romano, J. P. (1988). A bootstrap revival of some nonparametric distance tests. *Journal of the American Statistical Association*, *83*(403), 698–708.

Romano, J. P. (1989). Bootstrap and randomization tests of some nonparametric hypotheses. *The Annals of Statistics*, *17*, 141–159.

Ruhl, C. J., Abercrombie, R. E., Smith, K. D., & Zaliapin, I. (2016). Complex spatiotemporal evolution of the 2008 Mw 4.9 Mogul earthquake swarm (Reno, Nevada): Interplay of fluid and faulting. *Journal of Geophysical Research: Solid Earth*, *121*, 8196–8216. https://doi.org/10.1002/2016JB013399

Schaff, D. P., & Waldhauser, F. (2005). Waveform cross-correlation-based differential travel-time measurements at the Northern California Seismic Network. *Bulletin of the Seismological Society of America*, *95*(6), 2446–2461. https://doi.org/10.1785/0120040221

Schoenball, M., Davatzes, N. C., & Glen, J. M. (2015). Differentiating induced and natural seismicity using space-time-magnitude statistics applied to the Coso Geothermal field. *Geophysical Research Letters*, *42*, 6221–6228. https://doi.org/10.1002/2015GL064772

Schoenball, M., & Ellsworth, W. L. (2017). Waveform-relocated earthquake catalog for Oklahoma and southern Kansas illuminates the regional fault network. *Seismological Research Letters*, *88*(5), 1252–1258. https://doi.org/10.1785/0220170083

Schoenberg, F. P. (2003). Multidimensional residual analysis of point process models for earthquake occurrences. *Journal of the American Statistical Association*, *98*(464), 789–795. https://doi.org/10.1198/016214503000000710

Seif, S., Zechar, J. D., Mignan, A., Nandan, S., & Wiemer, S. (2019). Foreshocks and their potential deviation from general seismicity. *Bulletin of the Seismological Society of America*, *109*(1), 1–18. https://doi.org/10.1785/0120170188

Shcherbakov, R., & Turcotte, D. L. (2004). A modified form of Bath's law. *Bulletin of the Seismological Society of America*, *94*(5), 1968–1975. https://doi.org/10.1785/012003162

Shcherbakov, R., Turcotte, D. L., & Rundle, J. B. (2005). Aftershock statistics. *Pure and Applied Geophysics*, *162*(6-7), 1051–1076. https://doi.org/10.1007/s00024-004-2661-8

Teng, G., & Baker, J. W. (2019). Seismicity declustering and hazard analysis of the Oklahoma–Kansas Region. *Bulletin of the Seismological Society of America*, *109*(6), 2356–2366. https://doi.org/10.1785/0120190111

Trugman, D. T., Dougherty, S. L., Cochran, E. S., & Shearer, P. M. (2017). Source spectral properties of small to moderate earthquakes in southern Kansas. *Journal of Geophysical Research: Solid Earth*, *122*, 8021–8034. https://doi.org/10.1002/2017JB014649

Utsu, T., & Ogata, Y. (1995). The centenary of the Omori formula for a decay law of aftershock activity. *Journal of Physics of the Earth*, *43*(1), 1–33. https://doi.org/10.4294/jpe1952.43.1

van Stiphout, T., Zhuang, J., & Marsan, D. (2012). Seismicity declustering, Community Online Resource for Statistical Seismicity Analysis, doi:https://doi.org/10.5078/corssa-52382934. Available at http://www.corssa.org.

Vasylkivska, V. S., & Huerta, N. J. (2017). Spatiotemporal distribution of Oklahoma earthquakes: Exploring relationships using a nearest-neighbor approach. *Journal of Geophysical Research: Solid Earth*, *122*, 5395–5416. https://doi.org/10.1002/2016JB013918

Vere-Jones, D. (1969). A note on the statistical interpretation of Båth's law. *Bulletin of the Seismological Society of America*, *59*(4), 1535–1541.

Waldhauser, F., & Schaff, D. P. (2008). Large-scale relocation of two decades of Northern California seismicity using cross-correlation and double-difference methods. *Journal of Geophysical Research*, *113*, B08311. https://doi.org/10.1029/2007JB005479

Zaliapin, I., & Ben-Zion, Y. (2013a). Earthquake clusters in Southern California I: Identification and stability. *Journal of Geophysical Research: Solid Earth*, *118*, 2847–2864. https://doi.org/10.1002/jgrb.50179

Zaliapin, I., & Ben-Zion, Y. (2013b). Earthquake clusters in Southern California II: Classification and relation to physical properties of the crust. *Journal of Geophysical Research: Solid Earth*, *118*, 2865–2877. https://doi.org/10.1002/jgrb.50178

Zaliapin, I., & Ben-Zion, Y. (2015). Artefacts of earthquake location errors and short-term incompleteness on seismicity clusters in Southern California. *Geophysical Journal International*, *202*(3), 1949–1968. https://doi.org/10.1093/gji/ggv259

Zaliapin, I., & Ben-Zion, Y. (2016a). A global classification and characterization of earthquake clusters. *Geophysical Journal International*, *207*(1), 608–634. https://doi.org/10.1093/gji/ggw300

Zaliapin, I., & Ben-Zion, Y. (2016b). Discriminating characteristics of tectonic and human-induced seismicity. *Bulletin of the Seismological Society of America*, *106*(3), 846–859. https://doi.org/10.1785/0120150211

Zaliapin, I., Gabrielov, A., Keilis-Borok, V., & Wong, H. (2008). Clustering analysis of seismicity and aftershock identification. *Physical Review Letters*, *101*(1), 1–4.

Zhuang, J., Ogata, Y., & Vere-Jones, D. (2002). Stochastic declustering of space-time earthquake occurrences. *Journal of the American Statistical Association*, *97*(458), 369–380. https://doi.org/10.1198/016214502760046925